MASTER THESIS

# Understanding Sn-seeded InSb nanowire growth

*Author:*
Hengfang ZHANG

*Supervisors:*
Jonas JOHANSSON
Sebastian LEHMANN
Sepideh Gorji GHALAMESTANI

Division of Solid State Physics
Department of Physics

May 12th, 2017


LUND
UNIVERSITY

*"If you can't explain it simply, you don't understand it well enough."*

Albert Einstein

# Abstract

III-Sb semiconductor nanowires have drawn a lot of attention because of their many promising applications, such as thermoelectric generation, low power high efficient electronics and quantum transport. Gold as a catalyst seed particle has been dominating for many years assisting nanowires growth. However, gold is incompatible with silicon based electronics, which is dominating today. Therefore, finding metals alternative to gold as catalyst seed particles for III–V semiconductor nanowire growth is necessary. Sn was chosen as a promising seed particle for InSb nanowires growth.

The most commonly used bottom - up method is the Vapor - Liquid - Solid (VLS) mechanism. This project consisted of both experimental and theoretical components, with the aim to develop growth of InSb semiconductor nanowires using Sn droplets and Metal Organic Chemical Vapour Deposition (MOCVD). The composition of the Sn seeded InSb nanowires (including the seed particle) were determined by X-ray energy dispersive spectroscopy (XEDS). The morphology was characterized by scanning electron microscopy (SEM). Sn-seeded InSb nanowires growth was also discussed from a thermodynamic viewpoint using the phase diagram.

The optimized growth temperature was found to be $420°C$. The growth rate is low. Due to sample edge effects, the morphology of the nanowires (excluding the seed particle) is different between center and edge of the sample. The resulting InSb nanowires are much thicker (450 nm) and shorter (450 nm) compared to gold-seeded InSb nanowires. The nucleation and polarity of Sn-seeded InSb nanowires are more affected by V/III ratio than temperature. Particle size is strongly influenced by TMIn flow. The Sb amount is a key factor to control the morphology of InSb nanowires. We conclude that Sn-seeded InSb nanowires growth results in self-seeded (In) seeded InSb nanowires growth. The reasons are: 1). The seed particle size increases much during nanowires growth, from about 150 nm to 403 nm; 2). There is no significant effect on particle size with smaller seed particles growth; 3). XEDS measurements show that no Sn is detected. Mass transport modelling fits the experimental data of TMIn series much better than TMSb series. Further experiments on InSb nanowires growth without Sn seed particles verified that Sn-seed particles help nucleation and affect the InSb NWs growth.

# *Acknowledgements*

I have been so lucky to participate this thesis project. I would express my sincere thanks to all the people who helped and supported me on the way.

First of all, I would like to give my special thanks to my main supervisor, Dr. Jonas Johansson. Thanks for providing me the chance of doing this project. Thank you for always finding time for me, for your endless patience. Thank you for all suggestions and discussions about nanowires growth. Thanks for all your support.

I would like to thank my excellent assistant supervisors Dr. Sepideh Gorji Ghalamestani and Dr. Sebastian Lehmann. I could not finish the experiments without you. Thank you Sepideh for teaching me how MOVPE, SEM work and also about ImageJ and Microsoft Excel. Thank you Sebastian for your discussions and experimental support.

I would like to thank Prof. Kimberly Dick Thelander for giving me the opportunity to participating in research group meetings. I have always been inspired by your unimaginable knowledge and all other group members' talent.

I gratefully acknowledge Marcus Tornberg. Thank you for teaching and helping me with XEDS. Thank you also for showing me how to process images.

I would like to thank Dr. Zhaoxia Bi, Zhen Li and Xulu Zeng. Thank you for teaching me to use SEM, for your study guide.

Dr. Masoomeh Ghasemi is gratefully acknowledged for teaching me Thermo-Calc, for discussing the phase diagram.

I would like to thank Dr. Dan Hessman and Dr. Claudio Verdozzi. Thank you Dan for listening my thoughts and giving me valuable advice. Thank you Claudio for your tolerance and understanding of my special circumstances.

I would like to thank the members of Kimberly's research group for all the weekly meetings and scientific discussions: Dr. Sebastian Lehmann, Dr. Sepideh Gorji Ghalamestani, Marcus Tornberg, Erik Mårtensson, Luna Namazi, Robert Hallberg, Rong sun, Dr. Martin Ek, Dr. Hanna Kindlund, Dr. Reza Zamani, Dr. Karl Winkler, Magnus Dahl, Louise Gren.

I am grateful to my supportive and lovely friends for making my life in Lund colourful. I am proud of being your friend: Johan Ekström, Oskar Ström, Adam Jönsson, Chunlin Yu, Zhen Li, Rong Sun, Yian Wang, Yingjun Chen, Fangfang Yang, Mengqin Shen, Zheming Li, Genzhao Zheng, Qian Zhao, Baozhong Zhang, Ka Zhang, Tongchang Zhou, Yu Rui, Shaodong Jia, Xianyun Gao, Hongduo Lu, Fei Peng, Chu Zhang, Xulu Zeng.

Special thanks to my parents, parents-in-law, my brother, my sister for your unconditional support and encouragement over these years. Last but the most of all, thanks to my dear husband Mao Li and dear daughter Anna Jinxuan Li. I love you very much.

# Contents

# List of Abbreviations

| | |
|---|---|
| **Al** | **Al**uminum |
| **Ga** | **Ga**llium |
| **In** | **In**dium |
| **P** | **P**hosphorus |
| **As** | **Ars**enic |
| **Sb** | Antimony |
| **Sn** | Tin |
| **Au** | Gold |
| **InSb** | **In**dium Antimony |
| **TMIn** | Trimethylindium |
| **TMSb** | trimethylantimony |
| **TESn** | Tetraethyltin |
| **VLS** | **V**apor **L**iquid **S**olid |
| **MOCVD** | **M**etal **O**rganic **C**hemical **V**apour **D**eposition |
| **MOVPE** | **M**etal **O**rganic **V**apour **P**hase **E**pitaxy |
| **XEDS** | **X**-ray **E**nergy **D**ispersive **S**pectroscopy |
| **SEM** | **S**canning **E**lectron **M**icroscopy |
| **FSEM** | **F**ield emission **S**canning **E**lectron **M**icroscopy |
| **TEM** | **T**ransition **E**lectron **M**icroscopy |
| **ZB** | **Z**inc**B**lende |
| **BSE** | **B**acks**c**atter **E**lectron |
| **SE** | **S**econdary **E**lectron |
| **SCCM** | **S**tandard **C**ubic **C**entimeter per **M**inute |

# Chapter 1

# Introduction

## 1.1 Nanowire state-of-the-art

In today's nanoscience, a lot of results on the applications of semiconductor materials emerge. One of the most important applications of semiconductors is in electronics, since the Fermi level can be modified (by doping with impurity atoms), enabling tailoring of the electronic properties of semiconductors.

III-V semiconductors are compound semiconductors which combine of group III (Al, Ga, In, etc.) and group V (P, As, Sb, etc.) elements, For example, GaP, AlAs and InSb. These materials have direct band gaps. Photons can easily be generated by the recombination of electrons and holes from the conduction and valence bands. This property makes the III-V semiconductor materials interesting for optical applications. Indium antimonide (InSb) is a III–V compound semiconductor well known for its quite narrow band gap (0.163 eV at 300 k) and very high electron mobility ($7.7 \times 10^4 cm^2 V^{-1} S^{-1}$ ) [1].

Nanowires can be defined as one-dimensional structures with diameters in the range of tens of nanometers, and the third dimension much longer, typically in the range of micrometers [2]. There are few aspects to control for successful nanowire synthesis, such as nanowire morphology, composition, diameter, and electronic properties [3]. III-V semiconductor nanowires help developing fundamental physics and are promoting new applications in quantum electronics and optoelectronic devices[3]. III-V semiconductor nanowires can be fabricated by two general approaches: top-down and bottom-up [2] [3]. The top-down method starts from bulk substrate material and then nanowires are patterned through combinational processes of lithography and etching or milling. In contrast, the bottom up method nanowires are formed by self-assembly. The growth parameters can be controlled and tuned during nanowires synthesis. This method is much more flexible, and can be used for complex device fabrication. The most commonly used bottom-up method is Vapor-Liquid-Solid (VLS) mechanism based on Metal Organic Chemical Vapour Deposition (MOCVD) for nanowire synthesis. For detail of the MOCVD method and the VLS mechanism, we refer to the theory part in section 2.3.

The VLS is a fundamental nanowire growth method. The VLS model, which was developed over 50 years ago, is the key root technique adopted for nanowires growth nowadays. The metal seeded particle plays a fundamental aspect in this growth mechanism. Gold as a catalyst seed particle has been dominating for many years due to its several advantages [4] [5] [6]. First, the moderate melting point and formation of low-melting alloys of gold makes it a suitable and widely used seed particle material for

nanowire growth. Second, Gold as catalyst cannot easily oxidise and chemically stabilize during the growth processing. Third, it has very low electrical contact resistance that can be used when making devices. However, gold as catalyst seed particle also has some disadvantages. Gold introduces for example deep doping level in the band gap. It has a high solid diffusivity in silicon, these effects make gold as seed particle material incompatible with silicon based devices [6]. Because gold can form mid-gap electronic states in silicon, it is a forbidden element in complementary metal oxide-semiconductor (CMOS) devices particularly [5]. Additionally, gold is very expensive, which is not good for widespread commercial use and cost reduction.

Silicon is a technically important semiconductor which is favored in microelectronics industry. Apart from its commercial low-cost production, due to its natural abundance and native oxide and superior temperature performance [2], silicon has a wide range of applications. As mentioned above, although gold as seed particle has its advantages, its disadvantages can also not be ignored. Therefore, finding metals alternative to gold as catalyst seed particles for III–V semiconductor nanowire growth is necessary. Dick et.al. [5] reviewed the progress of III-V semiconductor nanowires using gold-free bottom-up synthesis techniques with alternative seed particles. Various foreign metals have been developed as seed particles to form III-V semiconductor nanowires, such as nickel, palladium, platinum, manganese, silver, copper, bismuth and iron [5]. Until now, only a few reports are known using (Sn) as seed metal for nanowires growth [7] [8] [9].

## 1.2 Indium antimonide (InSb)

The InSb compound semiconductor is an interesting material for transport physics and high speed electrics. The crystal structure of InSb is zincblende (ZB). The indium terminated {111} surface is called InSb {111}A surface (oriented along a [111] direction) and the antimony terminated one is called InSb {111}B surface (oriented along a [-1-1-1] direction) [10]. The compound has a well-defined atomic ratio In:Sb=1:1. Thus each In atom is tetrahedrally bonded to four Sb atoms in the bulk and vice versa [11]. On the InSb {111}B surface, the antimony (Sb) atom has two free electrons (five valence electrons in total) and can generate a pair of electrons in the bulk of the InSb semiconductor. In contrast, on InSb {111}A surface, Indium (In) atom has three valence electrons forming a vacancy. In oxide property, InSb {111}B surface is more active and easily oxided than the InSb {111}A surface [10].

There are many applications for InSb semiconductor nanowires. Mid-infrared photodetectors fabricated by single-crystal InSb nanowires are based on a metal semiconductor metal structure [12]. A gas sensor made by N-type InSb nanowires can detect nitrogen dioxide ($NO_2$) at room temperature [13]. In low-power high speed electronic devices, InSb nanowires are widely used as components [14]. One-dimensional transport (conductance quantization) in InSb nanowires at nonzero magnetic fields was reported by Ilse et al. [15]. Electronic transport properties of InSb have been investigated, while the applications of InSb for thermoelectric has also been developed [14] [16] [17].

InSb nanowires synthesis techniques are summed by Shafa et. al [4]. These techniques include MOCVD, Evaporation, Molecular Beam Epitaxy (MBE), Chemical Beam Epitaxy (CBE), and Solution-Based Techniques. With these various synthesis techniques, which method will be adopted depends on the goal to achieve or the desired

application, such as fabrication of a specific device. Nanowire epitaxy can be controlled in diameter, length and orientation very precisely using VLS synthesis technique. This project uses metal organic vapor phase epitaxy (MOVPE) technique for InSb nanowires growth.

InSb nanowires synthesis using MOVPE is enhanced by a metal droplet catalyst. By adopting MOVPE technique, high quality InSb nanowires can be achieved with gold as a catalyst seed particle [18] [19] [20]. However, a main drawback of the gold seed particle is that the interface energy of Au-InSb droplet is very high, which is not suitable for InSb nanowire nucleation. Gold also creates deep defects into InSb nanowires [4]. Considering some other disadvantages of using gold seed particle as mentioned above, it is necessary to discover the alternative metals as seed particles for InSb nanowires synthesis. $SiO_2$ as catalyst using MOCVD methods for InSb nanowires growth is reported by Lin [21]. Self-seeded InSb nanowires growth by MOCVD was successfully attempted in different substrates [22] [23] [24]. Sn as catalyst seed particle assisting InSb nanowires synthesis has not been reported yet.

## 1.3 Tin (Sn)

Tin (Sn) is a group IV element with atomic number 50 and tetragonal crystal structure. Sn has a low melting point at 505.08 K ($231.93^oC$), but high boiling point at 2875 K ($2602^oC$) at atmospheric pressure. Tin is well known for its allotropes and presents a semiconducting and thermodynamically stable diamond structure phase ($\alpha - Sn$) below $13.2^oC$, while it transforms to a metallic phase ( $\beta - Sn$) above $13.2^oC$ [25]. Sn grows in a layer-by-layer fashion on InSb {111} substrate as reported by Magnano [25]. It was shown that Sn occupies the In vacancies of the InSb surface, resulting in a $(1 \times 1)$ symmetry characteristic of pseudomorphic bulk-like Sn {111}.

Sn represents an amphoteric dopant in binary semiconductors. It behaves as an electron donor when substituting a group III element, while it behaves as an electron acceptor when substituting a group V element. Sn as n-type or p-type dopant in semiconductor nanowires has been reported in literature [26] [27] [28]. F. Terra et al. [29] investigated the effect of Sn dopants on the properties of InSb microcrystals grown from vapor phase. At small concentrations, Sn impurity exhibits mainly donor properties. For Sn concentrations in the range of $2 \times 10^{16} - 5 \times 10^{18} cm^{-3}$, it corresponds approximately to the 5:1 ratio of Sn atoms in In and Sb sub-lattices. A following increase of Sn concentration, will results in decrease of free electrons and in the electron mobility, which makes the resistivity of InSb to increase.

Sn as catalyst for nanowire growth has been reported in literature. Zamchiy [7] used plasma enhanced chemical vapor deposition technique to growth $SiO_2$ nanowires with Sn as catalyst seed particle. Sun [8] used Sn as a seed material for GaAs nanowires grown by MOVPE technique. Tornberg [9] demonstrated Sn-seeded GaSb homo- and GaAs–GaSb heterostructural nanowires by MOVPE technique. In and Sn alloy droplets as seed particles have also been reported to assist silicon nanowire growth [30] [31]. Sn particle seeded supercritical fluidliquidsolid synthesis of silicon nanowires with trisilane reactant was reported by Chockla [32]. Sn thin films coated as catalyst for silicon nanowires growth were also studied [33] [34].

## 1.4 Goal of the project

Metal catalyst seed particles can be achieved either by ex situ deposition or in situ formation on the substrate. For example, aerosol particles or substrate patterning using lithography are ex situ deposition of particles. The time between the particle formation and the nanowires growth is flexible. In contrast, nanowire growth process follows immediately after in situ particles formation. Thus, using in situ methods one can avoid sample contamination or oxidation by ambience, which is especially important for antimony based nanowires. In situ deposition of Sn seed particles will be used in this project.

III-Sb semiconductor nanowires have drawn a lot of attention recently. These groups of nanowires are of specific interest for applications, such as thermoelectric generation, low power high efficient electronics and quantum transport [14]. This project will use Sn as a seed particle material to investigate the VLS mechanism for InSb nanowire synthesis using MOVPE technique. InSb {111} A/B substrates will be used to get direct nanowire synthesis without substrate-nanowire lattice mismatch. Growth precursors are trimethylindium (TMIn), trimethylantimony (TMSb) and tetraethyltin (TESn). During growth, parameters such as temperature, V-III ratio, growth time, particle size will be altered to tune the InSb nanowires diameter or length. Optimized growth condition for Sn seeded InSb nanowires growth is expected to be obtained. It is very important to understand the Sn particle formation related to epitaxial growth of InSb nanowires.

In the following, components of Sn seeded InSb nanowire (including particle) will be determined by X-ray energy dispersive spectroscopy (XEDS). The morphology will be characterized by scanning electron microscopy (SEM). In this project, thermodynamic properties of Sn seeded InSb nanowires will be explained through phase diagrams. A mass transport modelling will be built in order to give a further understanding of Sn seeded InSb nanowires growth.

# Chapter 2

# Theory

## 2.1 Surface diffusion

Due to a concentration gradient in the multiple phases of grow the species, atoms move by thermodynamic driving force. Atoms arriving from the ambient (inside the MOVPE reactor chamber) on the substrate surface diffuse along the surface. At high enough temperature, the adatoms could also re-evaporate after staying on the surface for a short resident time [35]. The transport of precursor materials near the substrate plays an important role in III-V nanowires growth by MOCVD. This could affect nanowire growth parameters, such as time, particle diameter and interwire spacing.

The adatom encounters other atoms on the surface through surface diffusion to nucleate or form a growing island (or cluster). Generally, there are two ways of surface diffusion. One is that nanowires can collect materials directly impinging onto the nanowire side facets and seed particle surface. The other is that nanowires can collect materials from the substrate surface within the collection area equal to a circle area (standing wire in the center and diffusion length L as the radius) [2]. These adatoms could diffuse through the surface into the three phase boundary (Figure 2.1) contributing to nanowire growth or diffuse directly into nanowires contributing to the growth. Their diffusion length will determine the distance they can reach. This surface diffusion could have an effect on nanowire growth direction and morphology based on mass transport [36]. The diffusion of adatoms both from the substrate surface and nanowire facets affects the formation of nanowire crystal by VLS growth model [37]. Typically, group III species have much longer diffusion length like In. Best epitaxial growth is often achieved for large diffusion length [35]. By using TMIn as precursor, In species plays an important role of surface diffusion on nanowire synthesis with the VLS model [38] [39] [40] [41].

## 2.2 Ostwald ripening

After the precursors (TESn) decompose, the Sn atoms start to nucleate and form droplets at the initial stage. Then the droplets evolve so as to minimize their surface to volume ratio and surface free energy. In this process, small particles capillary shift to the large particles due to their concentration gradient. Small particles will become smaller and disappear in the end while large particles will grow and become bigger. This process will stop when there is no concentration gradient between the particles anymore. The process of this coarsening results in reducing number of droplets but increasing the average particle size, known as Ostwald ripening [42].

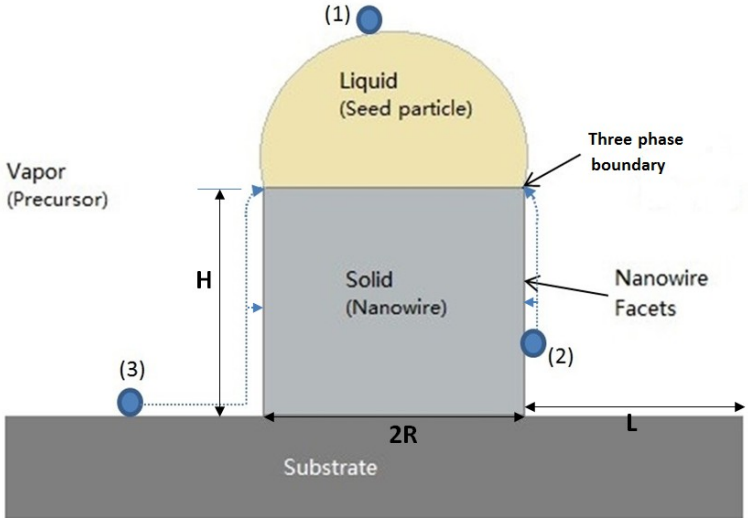


FIGURE 2.1: Illustration of VLS mechanism. The blue balls represent adatoms that impinge directly on the various surfaces: (1) on the seed particle, (2) on the nanowire facets (or sidewall), and (3) on the substrate surface. The dotted lines with arrows represent the paths of the adatoms for incorporation at the growth interfaces. Note: the proportion of seed particle, nanowire and substrate is not accurate, only used for illustration.

The application of Ostwald ripening to nanoparticles synthesis has been developed [43] [44] [45]. The density and the average radius of particles could be affected by certain parameters such as precursor source kinetics, formation time and temperature through thermodynamic properties. The distribution of Sn nanoparticles formed on the substrate can be broadened by the competition among Sn droplets leading to a more rapid coarsening rate.

## 2.3 Nanowire growth

### 2.3.1 Vapor-Liquid-Solid (VLS) growth mechanism

The VLS mechanism was first proposed by Wagner and Ellis [46] in 1964. From then on, this new method of nanowire growth started and it has been developed until now. Givargizov [47] detected the role of liquid phase by measuring the 'liquid phase effectivity coefficient' and showed that the activation energy was reduced by liquid phase both on Liquid-Solid interface (for nucleation) and Vapor - Liquid interface (for chemical reactions). Suppose the particle is a hemisphere on top of the cylinder nanowire (standing on the substrate surface) as shown in Figure 2.1. The metal organics (precursors) are carried with $H_2$ in the vapor phase. The Sn as seed particle is formed onto the substrate surface in liquid phase. The substrate is in solid phase and nanowire crystalline (InSb) is also formed in solid phase. The Vapor - Liquid interface is the surface area of hemisphere and the Vapor - Solid interface is the nanowire side facets marked in Figure 2.1. The Liquid - Solid interface is a circle area between seed particle and nanowire. Nanowires preferred to grow at the interface of Liquid - Solid and have much faster growth rate than other interfaces.

The Vapor - Liquid interface is a suitable site for deposition, because it has a large accommodation coefficient. Here, the accommodation is defined as an atom or molecule being incorporated from vapor phase into liquid phase or from vapor phase into solid phase. The accommodation coefficient is the fraction of being incorporated amount through phase transform rather than diffusing or desorbing [48]. The accommodation happens when growth species (In atoms and Sb atoms in this project) in the liquid cannot reach the state of supersaturation with respect to vapor phase. Nanowire growth occurs at the interface of Liquid - Solid when the liquid (seed particle) collects enough materials from vapor phase and becomes supersaturated ($\Delta\mu_{VS} > 0, \Delta\mu_{VS} = \mu_V - \mu_S$) [48]. The supersaturation ($\Delta\mu_{VS}$) is defined as the difference of chemical potentials between the atomic species in precursor vapor phase ($\mu_V$) and crystalline nanowire solid phase ($\mu_S$) at certain temperature [52-53]. $\mu_L$ represents the chemical potential in seed particle liquid phase. During nanowires growth, the chemical potential relation among VLS phase is $\mu_V > \mu_L > \mu_S$ [48].

### 2.3.2 Axial and radial growth modes

For particle assisted nanowire growth by MOVPE, there are two major growth modes: axial and radial growth. Mainly, they result in different directional growth. Axial growth is along the nanowire growth direction (perpendicular to the substrate) which determines the nanowire length. Radial growth is perpendicular to the nanowire growth direction (parallel to the substrate) which determines the nanowire diameter.

There are two major ways to axial growth mode [3]. One way is that reaction species can be collected from vapor phase to the liquid seed particle, which makes the nanowire growth happen at the Liquid - Solid interface as shown in Figure 2.1. The other way is that reaction species can be collected from adsorbed adatoms on the substrate or nanowire side facets. These adatoms diffuse along the concentration gradient toward the seed particle and contributing to the axial growth. However, the radial growth is also known as Vapor – Solid growth mechanism leading to the deposition of materials on the nanowire side facets. In this case, reaction species are also collected from adatoms on the substrate or nanowire side facets. Thus, the axial and the radial growths compete with each other in the progress of nanowire growth. Surface diffusion plays an important role in axial and radial growth [2]. Plante [49] described the growth of III–V nanowires from metal seed particles in the framework of a material conservation model. The diffusion length of adatoms distinguishes the axial the radial growth. A atomic step-mediated growth is included to describe the axial evolution of the shell [49].

### 2.3.3 Nucleation and Gibbs free energy

Initially, after the precursors are introduced, particles will be formed on the substrate. Nucleation is the first step of phase transformation. In the nanowires growth case, nucleation happens at the interface of initial phases between the metal seed particle and semiconductor. In this case, the new stable phase will be formed at supersaturation by consuming certain energy, based on the surface energy $\gamma$ of each phase. Thermodynamically, a nucleus is created by a change of Gibbs free energy $\Delta G$. Once the $\Delta G$ gets

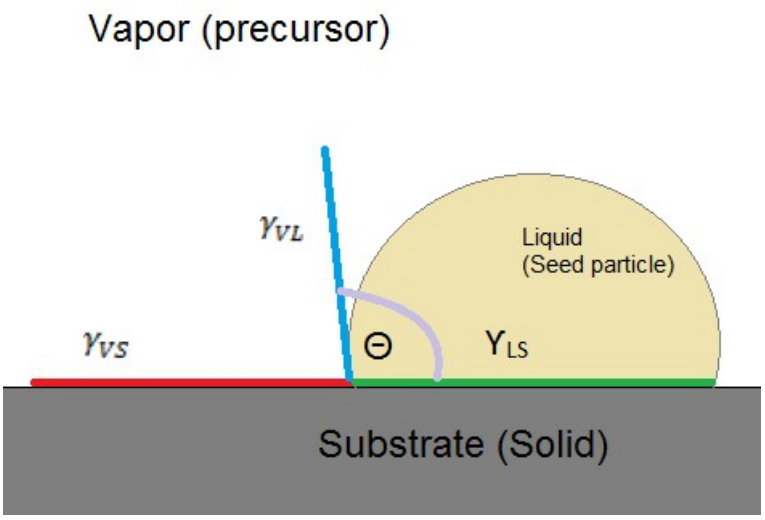


FIGURE 2.2: Illustration of wetting angle Θ balanced by surface energies. $\gamma_{VS}$ is the surface energy of Vapor-Solid interface; $\gamma_{LS}$ is the surface energy of Liquid-Solid interface; $\gamma_{VL}$ is the surface energy of Vapor-Liquid interface; Note: the proportion of seed particle, nanowire and substrate is not accurate, only used for illustration.

negative, the nucleus is stable. Then the growth of stable phase will not be limited by nucleation, but maybe factors such as diffusion and reaction kinetics.

The change of Gibbs free energy to form a crystalline nucleus at the interface of Vapor-Solid is written as follows:

$$\Delta G = -n\Delta\mu_{LS} + Ph\gamma_{LS} \tag{2.1}$$

$n$ represents the number of atoms or building blocks. The right first term is the energy needed for atoms transformed from liquid phase to Solid phase. At least the supersaturation equality is reached in the vapor and liquid, nucleation will occur in Liquid-Solid interface. Before the equality is achieved, the liquid seed particle will accommodate atoms or molecules from the vapor phase. The right second term represents the edge of nucleus with a small height h, perimeter length P and specific surface energy of Liquid-Solid interface ($\gamma_{VS}$). The other three interfaces have the same nucleus area [48].

In order to determine the different surface energies $\gamma$, wetting angle Θ of seed particle on the substrate will be measured. The balance of interface energies is given by Young's relation:

$$\gamma_{VS} = \gamma_{LS} + \gamma_{VL}cos\Theta \tag{2.2}$$

The wetting angle Θ can vary from $0^o$ to $180^o$ shown in Figure 2.2. There are three different growth modes corresponding to different wetting angle regions. When the wetting angle Θ belongs to [$0^o$, $90^o$] ($\gamma_{VS} \geq \gamma_{LS} + \gamma_{VL}$), meaning the material atoms are more strongly attracted on the substrate than themselves, then 2D layer-by-layer growth known as Frank-Van der Merve growth mode proceeds. If the material atoms prefer to strongly gather together themselves, the wetting angle belongs to [$90^o$, $180^o$] ($\gamma_{LS} \leq \gamma_{VL} + \gamma_{VS}$), meaning that the Liquid-Solid interface energy is very large or even

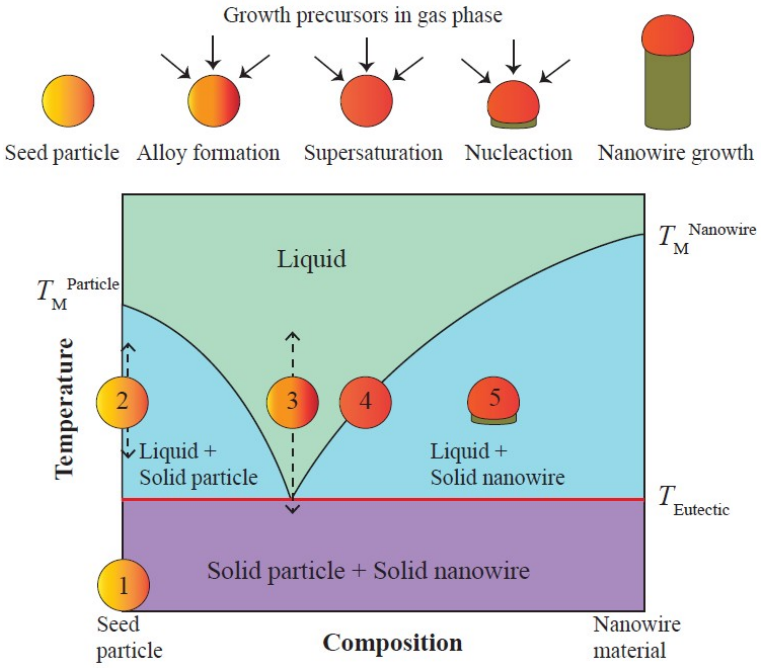


FIGURE 2.3: VLS growth mechanism in the view of phase diagram. Numbers point out the phase transformation for nanowire growth. They correlate to the growth processes on top of the figure. $T_M^{Particle}$, $T_M^{Nanowire}$ and $T_{Eutectic}$ denote the melting points of the seed particle, the nanowire material(s) and the eutectic point, respectively. By Ghasemi, M [50].

larger, then 3D island growth known as Volmer-Weber growth mode proceeds. Normally, the intermediate case is layer-plus-island growth known as Stranski-Krastanow growth mode. In this case, the wetting angle changes when the interface energies change during growth. Nucleation prefers occur at large wetting angles [48].

## 2.4 In-Sb-Sn ternary phase diagram

For the VLS nanowire growth mechanism, Ghasemi [50] gives the view in the form of phase diagram. For Vapor-Solid-Solid (VSS) nanowire growth, the seed particle is normally in solid phase (number 1, Figure 2.3) during nanowires growth. However, for VLS nanowire growth, the seed particle is typically in the liquid phase during nanowires growth. After the seed particles are formed, temperature sets at constant, but the phases transform from number 2 to number 5 (Figure 2.3)during nanowire growth. Arrow in number 2 indicates that seed particle can range in a temperature window such as annealing before nanowire growth. Growth precursors (TMIn, TMSb) in gas phase are kept at constant flow. By dissolving the growth species, alloy is usually formed (number 3, Figure 2.3) in liquid phase above the eutectic point. Arrow in number 3 denotes the shift of growth temperature depending on the growth materials. When supersaturation is reached in the seed particle (number 4, Figure 2.3), nucleation will take place and the nanowire (number 5, Figure 2.3) starts to grow.

In-Sb-Sn ternary phase diagrams are shown in Figure 2.4. The a) in Figure 2.4 is

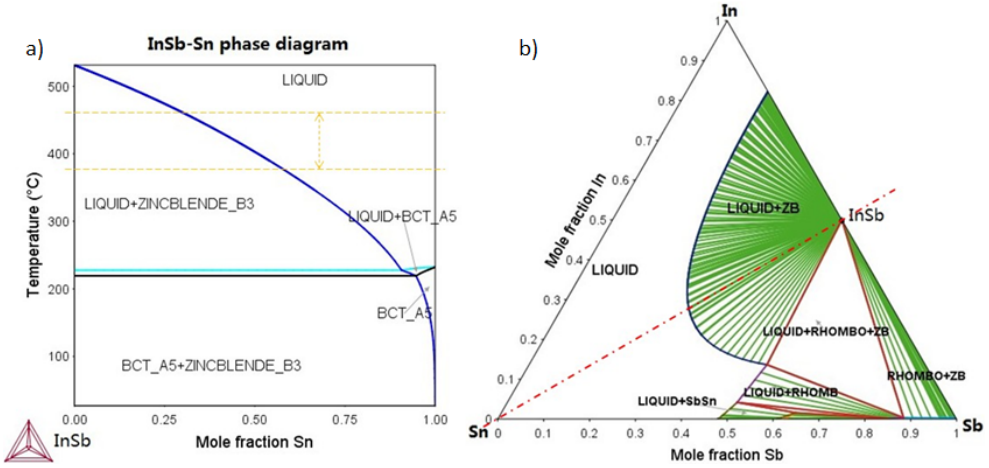


FIGURE 2.4: a). Sn-InSb binary phase diagram. b). In-Sb-Sn ternary phase diagram. Both dashed lines in figure a) (yellow) and b) (red) do not contribute to the construction of the phase diagram. In a), the phase diagram was drawn in the condition that the mole fraction of In and Sb is equal. Figure a) relates to the red dashed line (cut line) in Figure b). The region between two yellow dashed lines in a) indicates the temperature window of InSb nanowire growth. Temperature set is $420^oC$ in b). ZB represents zincblende phase and RHOMBO represents rhombohedral phase. Both a) and b) are calculated and plotted using Thermo-Calc.

plotted in the similar form as Figure 2.3 which is the prominent characteristics of eutectic type. The schematic of Sn-InSb binary phase diagram (Figure 2.4 a)) represents eutectic type behavior of the Sn-InSb. The eutectic point is about 95% Sn at $220^oC$. In comparison with Figure 2.3, we consider the conditions for Sn seeded InSb nanowire growth. The temperature range of InSb nanowire growth is set from $360^oC$ to $460^oC$ (dashed yellow lines in Figure 2.4 a)). There are two points considered. One is the decomposition temperatures of precursors (TMIn and TMSb) and the other is the melting point of InSb substrate. Supersaturation can happen near the blue line in Figure 2.4 a)(Liquid + ZB phase) within temperature region of growth. Thus it could indicate that the mole fraction of Sn in the seed particle ranges from 0 to 0.6 approximately. In common case of gold seed particles, the composition is AuIn or $AuIn_2$ for InSb nanowire growth [14]. However, it should be noticed that the measured compositions are performed at room temperature which is far away from the growth temperature. Many reactions can happen during cooling down, so that measured compositions cannot be exactly corresponding to the growth temperature. But we could assume this post-growth composition close to the supersaturated composition during growth. The biggest green area in Figure 2.4 b) is the two phase region with Liquid and ZB phases. It implies the composition of seed particle. This is the driving force that makes the InSb nanowires form.

## 2.5 InSb {111} surface reconstruction

Many surfaces of III-V compound semiconductors are polar. Their surface structures can be changed with composition and temperature. Surface reconstruction refers to

the process by which atoms at the surface of a crystal assume a different structure than that of the bulk. It could change as the vary of surrounding such as temperature, combined materials and so on. It is interesting to discover surface reconstructions. The reconstructions can be explained by orbital rehybridization and depolarization of the surface [51]. Due to the unsaturated dangling bonds on the surface, the surface atoms exhibit much more reactivity than those in the bulk. Many physical or chemical reactions take place on the surface. Especially for semiconductor nanowires that have a high surface to volume ratio. The surface takes an important part for nanowire growth, such as epitaxy.

Generally, InSb {111} A,B-$(2 \times 2)$ surfaces have been observed by ultrahigh vacuum high-resolution transmission electron microscopy [52], reflection high-energy electron diffraction [53], synchrotron X-Ray diffraction [54] and scanning tunnelling microscopy [55].

The InSb {111} A-$(2 \times 2)$ surface, can be described using an In-vacancy buckling model. There is a complete charge transfer from the In-atom of the outermost surface to the Sb atom of the second layer. $(2 \times 6)$ surface reconstruction exists under Sb rich condition between $200^oC$ to $230^oC$and completely changes to $(2 \times 2)$ surface above $260^oC$ [56] [57] [58]. Nakada found the transformation of a Sb-stabilized $(2 \times 6)$ surface into an In-stabilized $(2 \times 2)$ surface at $300^oC$ and the formation of Indium particles happened at $450^oC$ [59].

The InSb {111} B-$(2 \times 2)$ surface can be described by a Sb-trimer model. There is an incomplete charge transfer from Sb-trimer on the surface to the rest-Sb atom from the bulk [55]. A $(3 \times 3)$ reconstruction was observed by Wever in ultra-high vacuum under several hours annealing at $400^oC$ [51] or $427^oC$ [60]. A highly ordered $(3 \times 1)$ symmetry reconstruction was discovered around $477^oC$ just under the melting point of InSb $(547^oC)$ [60]. Both $(3\times3)$ and $(3\times1)$ reconstructions are driven by the deficiency of Sb in the surface layer. By using reflection electron microscopy at $420^oC$ and under Sb-rich conditions, Nakada found the transformation of a Sb-stabilized $(2 \times 2)$ surface into an In-stabilized $(3 \times 1)$ surface, resulting in the formation of Indium particles around 0.5-3.0 $\mu m$ in diameter. Before the formation of Indium particles, Sb atoms in the second layer are desorbed first [59].

# Chapter 3

# Experimental Set-up

## 3.1 MOVPE

### 3.1.1 Precursor chemistry

The most common used precursor materials such as trimethylindium (TMIn), trimethylantimony (TMSb) and tetraethyltin (TESn) play an important role as vapor phase in semiconductor nanowires growth using the MOVPE method. Temperature always dominates the pyrolysis of these precursors. At low temperature, precursors are decomposed incompletely leading the nanowires to chemical reaction limited growth. While at the high temperature, precursors can be decomposed completely but leading nanowires to mass-transport limited growth. In generally, nanowires growth takes place in the low temperatures region [2]. Then it is important to understand the principle of precursor actions for nanowires growth.

This project will use $H_2$ as carrier gas for precursors. The pyrolysis of precursors TMIn and TMSb and will be enhanced by $H_2$[61] [62]. The enhanced pyrolysis in $H_2$ is attributed to radical attack by H on TMIn (chemical formula $In(CH_3)_3$) and TMSb (chemical formula $(CH_3)_3Sb$) [61] [62]. It takes mainly three steps for $In - CH_3$ bonds to break off through decomposition of TMIn. TMIn can be completely decomposed at low temperature $350^oC$ [61] [63]. TMSb decomposes completely in hydrogen with few chemical reaction steps at relatively high temperature $450^oC$ [62]. The decomposition is a very complex processing which contains several chemical steps. Decomposition mechanisms changes when combines TMIn and TMSb. TMIn and TMSb compete for H atoms to accelerate their pyrolysis rates. The addition of TMIn results in lower decomposition temperatures for TMSb. In other words, TMIn pyrolysis causes an increase in the TMSb pyrolysis rate [62]. TESn (chemical formular $(C_2H_5)_4Sn$) was used in many semiconductor nanowires synthesis as precursor source of dopant (Sn) [26] [27] [28]. According to Louise's [64] former study, the optimized conditions of Sn seed particles formation on InSb substrate were determined. That is TESn source flow setting at $3.6 \times 10^{-9}$ mol/min, time controlling in 15 minutes and temperature at $400^oC$. These conditions will be used for Sn particle in situ formation on InSb substrates in this project.

### 3.1.2 The MOVPE set-up

The MOVPE is a very complex process technique for crystal growth. There are several key processes during the MOVPE growth. The driving force for epitaxy, phase transformation, mass transport processes and rates are considered as thermodynamic

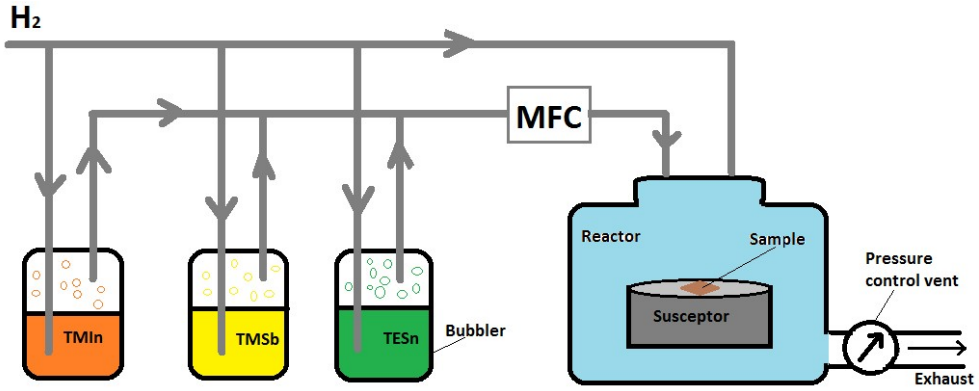


FIGURE 3.1: A simple schematic image of MOVPE system. The arrows indicate directions of the gases flow. The sample is placed on the heated susceptor inside the reactor where the nanowires growth takes place. The precursors flow rate is controlled by MFC (mass flow control). The reactor pressure is kept constant at 100 $mbar$ by pressure control vent.

processes. Reaction kinetics, surface reconstruction and diffusion are the physical surface processes. Pyrolysis of precursors and adsorption of products are the complex chemical reactions. Thus, even much more processes could happen during MOVPE growth. The reactor behaves like a black box which contains many complex precesses that cannot be described specifically. During the MOVPE growth experiment, we can control the salient features, such as temperature, reactor pressure, and mass flow of precursors. However, there are some limitations during the nanowires growth. The reactions mechanism can be limited by the pyrolysis and growth rates due to the low temperature and pressure region.

In this experiment, we use Aixtron MOVPE system of closed coupled showerhead (CCS) technology. A simple schematic image of the MOVPE system is shown in Figure 3.1. Three different precursors are used for Sn seeded InSb nanowires growth. They are metal organics TMIn, TMSb and TESn, which are mentioned in the theory part. The precursor sources are stored in the bubblers (Figure 3.1) at constant temperatures with $17^oC$ (TMIn), $10^oC$ (TMSb) and $17^oC$(TESn) respectively. These precursors are very dilute. Pure $H_2$ gas with constant flow rate will go into the bubblers down to bottom and then carry out precursors in gas phase through outlet of bubblers. Thus the constant temperatures of bubbles and $H_2$ gas flow rate are important for the evaporation of metal organics. The mass flow control (MFC) are used to control the flow rate of precursors stable and keep the total flow rate of the MOVPE system at constant. The blue box in Figure 3.1 is the reactor of the MOVPE system. This is a vertical reactor called CCS reactor just like a showerhead in the bathroom. The precursors are introduced in the carriers gas $H_2$ at the top of the reactor and are introduced perpendicularly to the susceptor surface. The susceptor (a material used for its ability to absorb electromagnetic energy and convert it to heat) is rotated in a constant low speed and heated by a resistance heater. Samples are set on the susceptor surface and rotated together with the susceptor. The showerhead design for incoming precursors and the set for rotating susceptor assure that the reactant species are distributed uniformly on the sample surface. The complex processes take place in this reactor such as chemical reactions, atoms diffusions, crystal epitaxy, and nanowires growth. The total pressure

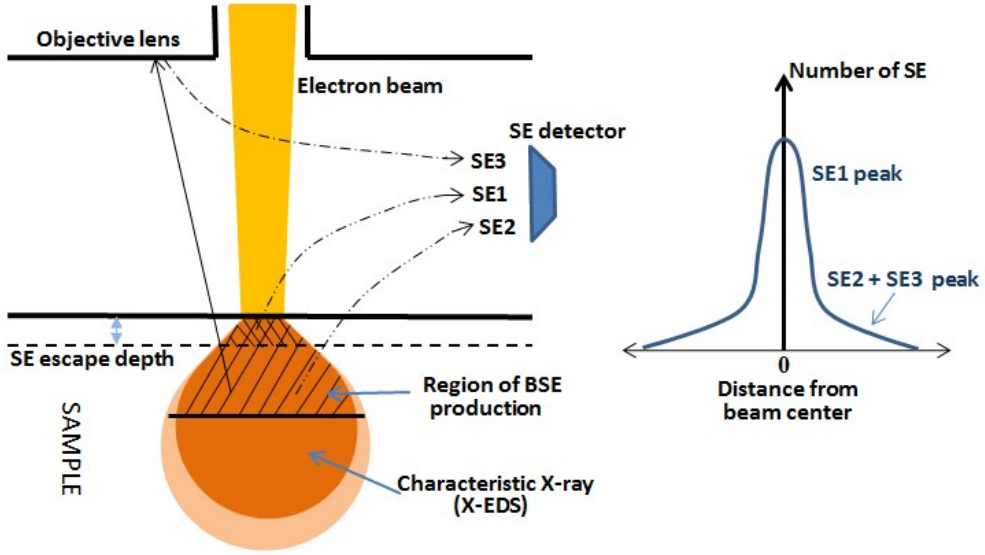


FIGURE 3.2: The drop-shape in the figure is the excitation volume when the incident electron beam interacts with sample. Most secondary electron (SE) comes from SE1. SE2 and SE3 contribute only small part for sample imaging.

of the system retains at 100 $mbar$. The pressure control vent controls the exhaust flow rate and keeps the pressure of reactor constant.

## 3.2 Electron microscopy

### 3.2.1 Scanning electron microscopy (SEM)

In this project, SEM in type of Hitachi SU8010 operated at 15 kV was used. SEM is a type of electron microscopy which produces topographical images of sample surface. A focused electron beam is scanned across the sample interacting with atoms in the sample. Typically, the focused electron beam is generated by tungsten thermionic type of electron gun. In SEM, the electron beam energy keeps in a low range (less than 50 $keV$). By proper parameters setting, a good SEM image can be obtained with high resolution. These parameters include astigmatism (aberration of electron lens), acceleration voltage (incident electrons), working distance (distance between beam aperture and sample) and sample tilt (angle between incident beam and sample).

Normally, there are two types of image detectors in SEM. One is secondary electron (SE) detector and the other is backscatter electron (BSE) detector. BSE detector is sensitive to sample composition which related to atomic number. BSE detectors are typically placed above the sample in the sample chamber based on the scattering geometry relative to the incident beam. Figure 3.2 shows the excitation volume which illustrates the path of electrons detected. The size of excitation volume depends on the accelerating voltage of incident beam electron and the atomic number of sample. When the incident beam interacts with sample, primary secondary electrons (SE1) are formed within a SE escape depth near the sample surface region. SE2 are created by backscattered electrons deep in the sample (shown in the region of BSE production).

SE3 are caused by backscattered electrons hitting other parts of the microscopy. SE detector can be side mounted (shown in Figure 3.2) or in-lens (not show in Figure 3.2) and only collects part of electrons that reach the detector grid. The right side image from Figure 3.2 shows the ratio of electron number between SE1 and SE2 plus SE3. As SE1 comes very near surface region (about 5 $nm$ to 50 $nm$ deep), the images obtained from SEM reflect the natural-looking topography of sample[65] [66]. In this project, we used SE detector from SEM to image nanowires and particles.

### 3.2.2 X-ray energy dispersive spectroscopy (XEDS)

XEDS is an analytical technique, which is used to determine the atomic composition in a sample. It is widely used to do chemical characterization of a sample. It relies on the interaction of incident electron beam and the sample. The source of the emission of characteristic X-ray is shown in Figure 3.2.

In a steady state, atoms have nucleus in the center bounded with unexcited electrons in discrete energy levels (electron shells). The incident electron beam can eject an electron at inner shell and create a hole at the same time. Then electron from outer shell at higher energy level will relax to fill the hole. The energy difference between the outer shell and inner shell may be released in the form of x-ray. The energy difference between two electron shells is unique in an atom. Due to a unique atomic structure, each element emits a characteristic set of discrete wavelengths (corresponding to emission energy). An energy-dispersive spectrometer can measure the emitted x-ray and can be mounted inside the chambler of a SEM or transimission electron microscopy (TEM). This results in XEDS spectrum. Most commonly, L shell energy may be detected [65] [66]. In this project, we use XEDS (mounted to SEM or TEM) to determine the element composition of Sn seeded InSb nanowires.

# Chapter 4

# Results and Discussion

In general, during an experimental process we changed only one parameter and kept the other parameters fixed at each experiment. Due to the very low vapour pressure of Sb, it is very easy to contaminate the reactor, which will affect the next growth run as well. Thus a cleaning run is executed between two growth runs. All the samples were set at one hour for growth. However, we also set a two hours growth for one sample. First, we ran a temperature series and found a best growth temperature at $420°C$. Second, we followed by V-III ratio series with sources TMIn and TMSb changing respectively. Another two runs about total flow changing (with fixed V-III ratio) gave the overview of the growth influence. Third, some particle formation samples were studied in order to get the particle sizes and densities before InSb nanowires growth. Fourth, except one hour growth, only two hours growth is performed. Fifth, through the XEDS analysis, the composition of particles and nanowires were determined. Finally, a mass transport model was built to simulate the growth rate versus source flow. This modelling will help us to understand how the nanowires grow. In the following discussion, there will be more specific details to be described.

## 4.1 Sn-seeded InSb nanowire growth on InSb {111}-type substrates

In this part, we focus on the results and discussion of the experiments epitaxial on Sn-seeded InSb nanowires growth. There are mainly three parts, which are temperature series, V-III ratio series, and time series. In the V-III ratio series, we divided the growth runs into three different sections. On each sample, three random central spots and three random edge spots were selected for the statistics. About 80 to 120 nanowires were measured on each sample. The measurements were executed by ImageJ software (an open source image processing program). These measurements are limited by accuracy of the software, human factor and also some other (image resolution, number of measurements...). Thus, the results of the measurements are sensitive to the statistical errors during data collection.

All the samples have the same recipe for Sn particle formation. The main parameters are TESn flow at $3.6 \times 10^{-9}$ mol/min, formation time at 900 second, real temperature at $409°C$. In each run, we loaded InSb {111}A and InSb {111}B substrates in the reactor. However, we did not find any nanowires on the InSb {111}B substrates. We only give the comparison growth of InSb {111}A and InSb {111}B substrates at temperature series. When we took SEM images of nanowires, we mostly used $30°$ sample

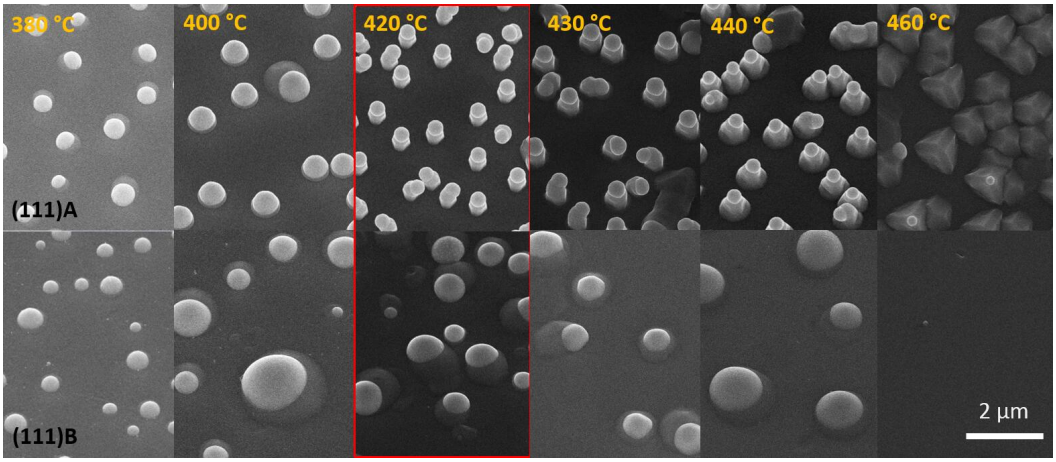


FIGURE 4.1: 30° tilted SEM images of Temperature series. Temperatures swept from $380°C$ to $460°C$. The first row shows that InSb nanowires grew on InSb {111}A substrates, while the second row was on InSb {111}B substrates. The red rectangular border is the preferred reference sample. The scale bar is shown at the right bottom

tilted to detect the nanowires morphology. However, there are also images taken in top view, which means that the electron beam is perpendicular to the sample.

### 4.1.1 Temperature series

Figure 4.1 shows the $30°$ tilted SEM images on temperature series. In this section, only the temperature varied and other parameters were kept constant such as TMIn source flow at $1.9 \times 10^{-9}$ mol/min, TMSb source flow at $4.8 \times 10^{-8}$ mol/min, V/III ratio at 25 and growth time at 1 hour. InSb nanowires grew in the temperature range of $420°C$ to $440°C$ on the (111)A substrate. This growth temperature is limited on one hand due to the relatively high temperature required for cracking the TMSb precursor and on the other hand by the low melting point of InSb ($527°C$) [22]. It should be noticed that increasing the temperature will cause an increasing cracking efficiency of the TMSb precursor (Refer to cracking temperatures of precursors in section 3.1.1), which leads to an increased effective V-III ratio. The surface diffusion length also increased as the temperature increase [67]. All these will have an effect on InSb nanowires growth. On (111)A substrate, only non-straight nanowires were found at lower temperature region ($380°C$ and $400°C$). A high yield of vertical and homogeneous nanowires are observed at $420°C$. When the temperature is increased, the tapered nanowires (or triangular pyramid islands) tend to form at the InSb {111} A substrate. High yield of vertical InSb nanowires have been observed above $430°C$ in gold-seeded nanowires growth by MOVPE [68]. Based on the In-Sb-Sn ternary phase diagram in Figure 2.4, the expected Sn composition is in the range of 0.36 to 0.45 in mole fraction.

However, on the InSb {111}B substrates, we notice that the density of nano-structures decreases (Figure 4.1) when the temperature increases. However, there are much less but bigger particles formed at higher temperature ($440°C$). This observation can be referred to the the phenomenon of Ostwald ripening. We observed very smooth surfaces on InSb {111}B substrate at $460°C$ which potentially is layer growth under this condition. No straight nanowires were found on InSb {111}B substrate, but only non-straight

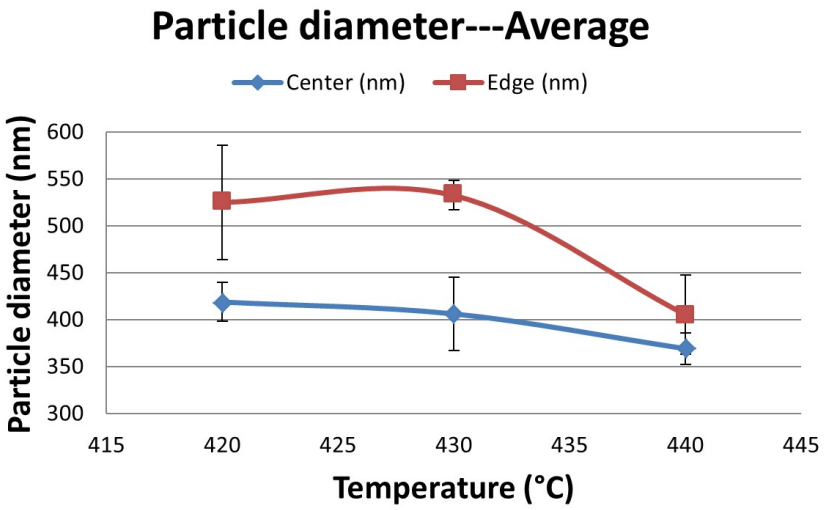


FIGURE 4.2: Temperature series–Average particle diameter. Blue and red squares are measured experimental data. Red and blue curves are guides for the eyes by measured data from centre and edge areas respectively. Vertical black solid lines with caps are error bars from standard deviation.

nanowires. The reason for this could be that InSb {111}B substrate is much chemically more active than InSb {111}A substrate which means that InSb {111}B substrate is easily oxidized [10]. There should be some extra steps for example chemical etching to remove oxides from the InSb {111}B substrate in order to grow epitaxial nanowires. The size distribution on InSb {111}A is much more uniform than it is the case on InSb {111}B substrates. The reasons could be related to different surface energies and surface structures on InSb {111}A and B. No InSb nanowires could be found on InSb(111)B by gold-seeded growth also[68].

In Figure 4.2 and Figure 4.3, the measured data both for particle diameter and nanowire length (excluding particle length) are shown. In this two figures, data were collected from three samples which were grown at $420°C$, $430°C$ and $440°C$ respectively. They were all from InSb {111}A substrates as we did not find any nanowires on InSb {111}B substrates. Red and blue squares in figures are measured experimental data, respectively. All the curves are guided to the eyes. The red curves give the data from central areas while the blue curves provide the data from edge areas. Thus, the average value should be the sum from center and edge areas which could be estimate from the curves. The values of the error bars are estimated from standard deviations. The average value of particle diameters tend to decrease as temperature increases as shown in Figure 4.2. The particle sizes have very big difference between center and edge and the difference decreased when the temperature is increased. The particle size is much bigger on the edge than it is on the center due to the substrate edge effect, which means a rough surface on the edge and that more atoms gather. However, for nanowire length in Figure 4.3, the tendency is opposite. The average values of nanowire length increase for higher growth temperatures. There are not so big variations between central and edge values compared to the particle diameter findings. It should be noticed that the particle diameters are very large which is about 400 nm to 540 nm compared to Au seeded particle sizes (20 nm to 100 nm). The nanowire lengths are around 550 nm which indicates that the growth rate is low. From the overview

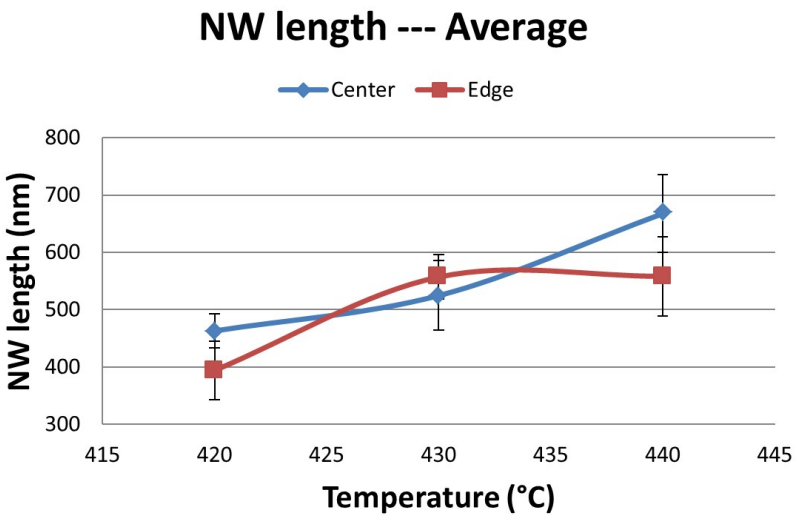


FIGURE 4.3: Temperature series–Average nanowire length. Blue and red squares with caps are measured experimental data from centre and edge areas respectively. Red and blue curves are guides for the eyes. Vertical black solid lines with caps are error bars corresponding to standard deviation.

discussion, we chose $420°C$ as the optimized temperature.

### 4.1.2 V/III ratio—TMIn flow series

In this section, we only varied TMIn molar flow and kept other parameters constant. Those were temperature at $420°C$, TMSb source flow at $4.8 \times 10^{-8}$ mol/min (15 sccm), growth time at 1 hour. The TMIn source flow were $4.9 \times 10^{-10}$ mol/min (9 sccm), $6.3 \times 10^{-10}$ mol/min (11.7 sccm), $9.5 \times 10^{-10}$ mol/min (17.5 sccm), $1.9 \times 10^{-9}$ mol/min (35 sccm) and corresponding to V/III ratio at 98, 75, 50 and 25 respectively. Thus, TMIn source flow increases when V/III ratio decreases. As we can see from Figure 4.4 and Figure 4.5, it is very obvious that TMIn source flow influences both the particle sizes

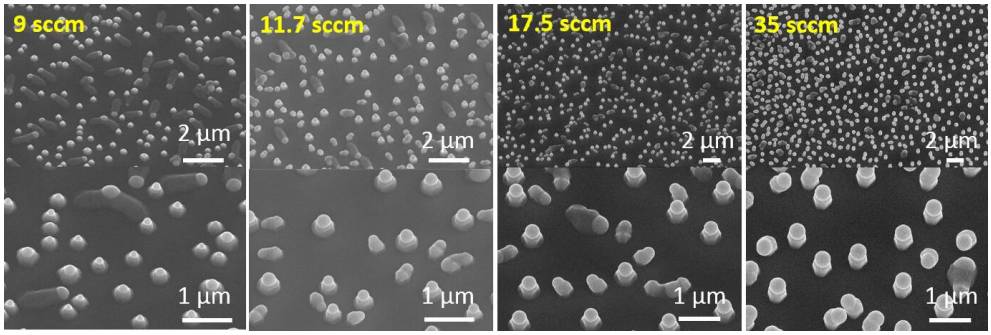


FIGURE 4.4: V/III ratio—TMIn series. The values of TMIn source flow are displayed on top left images in yellow fonts. All images were taken on InSb {111}A substrates in central parts by SEM with the sample tilted 30°. The second row images are magnified from top row images. Scale bars are shown at right bottom on each images.

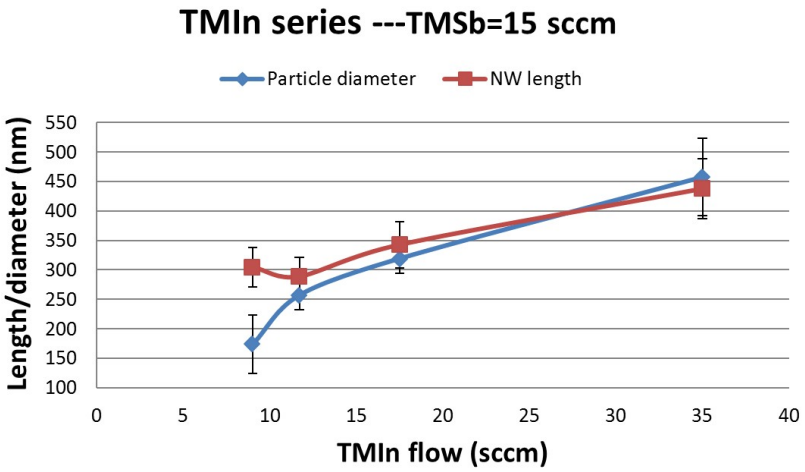


FIGURE 4.5: V/III ratio—TMIn series data. Blue and red squares are measured experimental data. Red curve is the average value of nanowire lengths. Blue curve is the average value of particle diameters. Red and blue curves are all guides for the eyes. Vertical black solid lines with caps are error bars from standard deviation.

and nanowire lengths at the same time. It seems that the nanowires growth rate scales with the TMIn molar flow. Especially the particle sizes are affected by TMIn source flow. From the experimental data of Figure 4.5, the diameter of particle is equal to the length of nanowires approximately as TMIn source flow varies. Lin [21] observed under indium-rich conditions self-seeded InSb nanowires growth with particle diameter of around 290 nm and lengths of nanowires of around 410 nm. Therefore, we assume that there is much indium inside the seed particles. The nanowire composition will be checked by XEDS characteristic.

### 4.1.3 V/III ratio—TMSb flow series

In the next set of experiments, we varied the TMSb source flow and kept the other parameters constant. These were temperature at $420°C$, TMIn source flow at $9.5 \times 10^{-10}$ mol/min (17.5 sccm), the growth time was 1 hour. The TMSb source flows were $2.4 \times 10^{-8}$ mol/min (7.5 sccm), $4.8 \times 10^{-8}$ mol/min (15 sccm), $9.5 \times 10^{-8}$ mol/min (30 sccm), $1.4 \times 10^{-7}$ mol/min (45 sccm), corresponding to V/III ratios of 25, 50, 100 and 150, respectively. Sb has a very low vapour pressure which makes it easy to stick to the epitaxial surfaces. Excess supply of Sb may lead to uncontrolled growth and even formation of Sb crystallites [14]. However, by using the MOVPE growth method, this parasitic route will become much more complicated with all the chemical reactions involved. About 50% TMSb is decomposed at $420°C$ [62]. Thus, the true V/III ratio is probably lower than the numerical value. Because of too many inclined wires, it was difficult to measure the nanowire lengths accurately. The green frame in Figure 4.7 indicates that the measured data are uncertain due to the morphology of the nanowires. Although most nanowires tend to bend when the TMSb source flow is increased, we could make sure that the length of the nanowires indeed increases through the observed SEM images (Figure 4.6). The diameter of particles does not seem to change

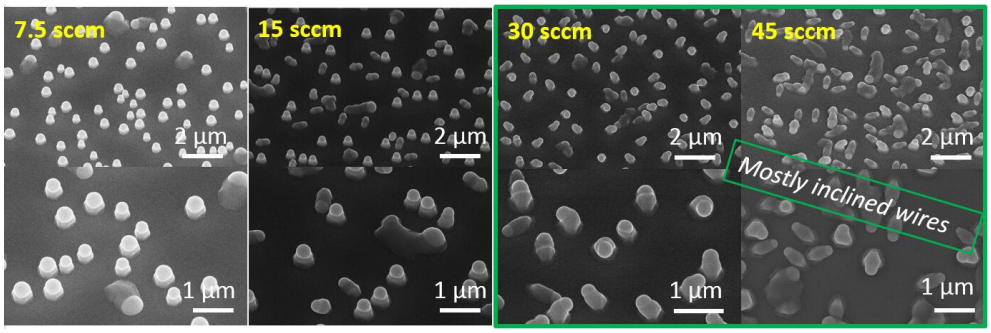


FIGURE 4.6: V/III ratio—TMSb series. TMSb source flow are displayed on top left images in yellow fonts. All images were taken on InSb {111}A substrates in central parts by SEM with the sample tilted 30°. The second row images are magnified from top row images. Scale bars are shown at right bottom on each images. The green frames gives the hint that nanowires are mostly inclined.

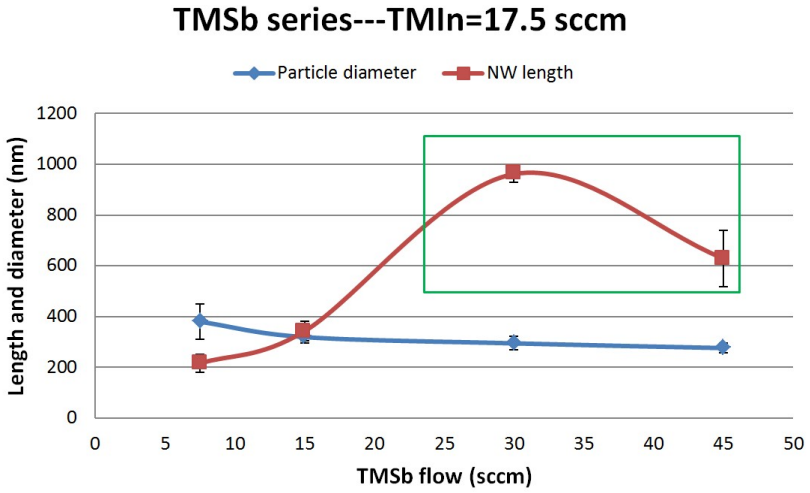


FIGURE 4.7: V/III ratio—TMSb series data. Blue and red squares are measured experimental data. Red curve is the average value of nanowire lengths. Blue curve is the average value of particle diameters. Red and blue curves are guides for the eyes. Vertical black solid lines with caps are error bars from standard deviation. The green frame correspond to Figure 4.6 and expresses that the measured data is uncertain due to the large fraction of inclined wires.

TABLE 4.1: Total flow series data

| Image NO. | TMIn flow | TMSb flow | Particle diameter | Nanowire length |
|---|---|---|---|---|
| Figure 4.8 a) | $1.9 \times 10^{-9}$ mol/min | $4.8 \times 10^{-8}$ mol/min | 458± 65 nm | 438± 51 nm |
| Figure 4.8 b) | $9.5 \times 10^{-10}$ mol/min | $2.4 \times 10^{-8}$ mol/min | 378±68 nm | 215± 35 nm |

whenever TMSb source flow is varied. We could predict that the amount of antimony give little affect on the diameter of the seed particles. However, the TMSb source flow effect the nanowire morphology and growth rate quite much. The optimal growth rate that could give a mostly axial growth is not observed at the current conditions.

Typically, for antimonide nanowires growth, the radial growth rate is group-III-limited, while the axial growth rate can be group-V-limited [14]. As V-III ratio increases shown in Figure 4.6, much more inclined nanowires and non-epitaxial InSb nanowires are observed, but the growth rate increases. In this case, the axial growth rate for InSb nanowires is dependent on the TMSb source flow up to a certain point (Figure 4.7, green box), after which it decreases. The axial growth rate strongly depends on the TMIn source flow as shown in Figure 4.4 and Figure 4.5. The radial growth relies on the diameter of the seed particle. A relatively high TMIn source flow results in significantly radial and axial nanowires growth, while a even lower TMIn source flow results in shorter, thinner and non-epitaxial nanowires growth.

As we can see from Figure 4.6 and Figure 4.7, it is obvious that the TMSb source flow has a big influence on the nanowire growth rate. However, it nearly has no effects on particle sizes. The green frames marked in Figure 4.6 give the notice that these nanowires are mostly inclined wires. The nanowires could grow from many different facets and there is no uniform direction as observed. This could be due to the surfactant effects of Sb. The Sb adatoms float on top of the growing layer without being incorporated. The reason for this could be that Sb is a relatively heavy atom (atom number 51) and has long covalent bonds. The Sb surfactant effect can also have a big influence on the inter-facial energies for the nanowires growth [14]. According to Du [69], this Sb atoms adsorption at Vapour-Liquid and Liquid-Solid interfaces make the inter-facial forces alter resulting in changing the wetting angle (Figure 2.2) and blocking or reducing the incorporation of atoms. This surfactant effect of Sb maybe the reason why the nanowires have so large diameter and the growth rate is so low. Therefore, it indicates that the Sb amount is a key factor in controlling the morphology of the nano-structures.

### 4.1.4 V/III ratio—Total flow series

The sample with high yield vertical and uniform nanowires is chosen as reference sample as shown in Figure 4.8 a). The optimized growth conditions are temperature at $420°C$, TMIn source flow at $1.9 \times 10^{-9}$ mol/min, TMSb source flow at $4.8 \times 10^{-8}$ mol/min, growth time at 1 hour, V-III ratio at 25. When we decreased both the TMIn source flow and TMSb source flow to half amount (with $9.5 \times 10^{-10}$ mol/min and

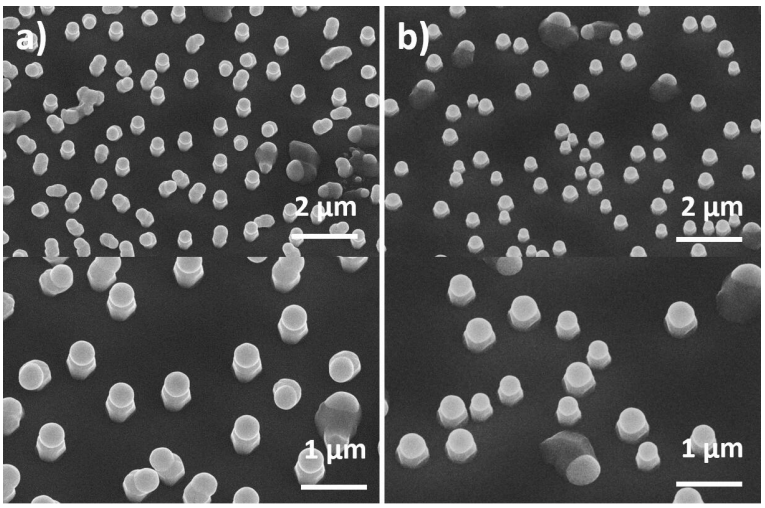


FIGURE 4.8: V/III ratio—Total flow. TMIn source flow and TMSb source flow are decreased both at the same time from reference sample a) (with TMIn flow=$1.9 \times 10^{-9}$ mol/min and TMSb flow=$4.8 \times 10^{-8}$ mol/min) to sample b)(with TMIn flow=$9.5 \times 10^{-10}$ mol/min and TMSb flow=$2.4 \times 10^{-8}$ mol/min). All images were taken on InSb{111}A substrates in central parts by SEM with the sample tilted $30°$. The second row images are magnified from top row images. Scale bars are shown at right bottom on each images.

TABLE 4.2: Time series data

| Image NO. | Particle diameter | NW length |
|---|---|---|
| Figure 4.9 1 h | 403± 68 nm | 376± 48 nm |
| Figure 4.9 2 h | 574± 36 nm | 1118± 210 nm |

$2.4 \times 10^{-8}$ mol/min respectively) as shown in Figure 4.8 b), the V-III ratio was still at 25. In this case, it means that we decreased the materials supply. The distribution of nanowire diameter becomes uniform when we decreased the material supply (Figure 4.8). The nanowire length decreased about half amount which also shown in Table 4.1.

### 4.1.5 Time series

For the 1 hour (1 h) sample, we chose the reference sample the same as Figure 4.8 a). The constant parameters are temperature at $420°C$, TMIn source flow at $1.9 \times 10^{-9}$ mol/min, TMSb source flow at $4.8 \times 10^{-8}$ mol/min, V-III ratio at 25. For another time series sample run, we only did 2 hours (2 h) growth. We planned to do more runs on time series, however, the outcome of Figure 4.9, 2 h growth was not expected. As we could see from the figure, there are much more kinked nanowires in 2 h growth. Although there are inclined nanowires, it is obvious that nanowire length indeed increases much. Table 4.2 gives the rough measurement, we could see that with 2 h growth nanowire length is at least two times as the same length as 1 h growth. Both diameter and length of nanowires increase as time increases. This result agrees with

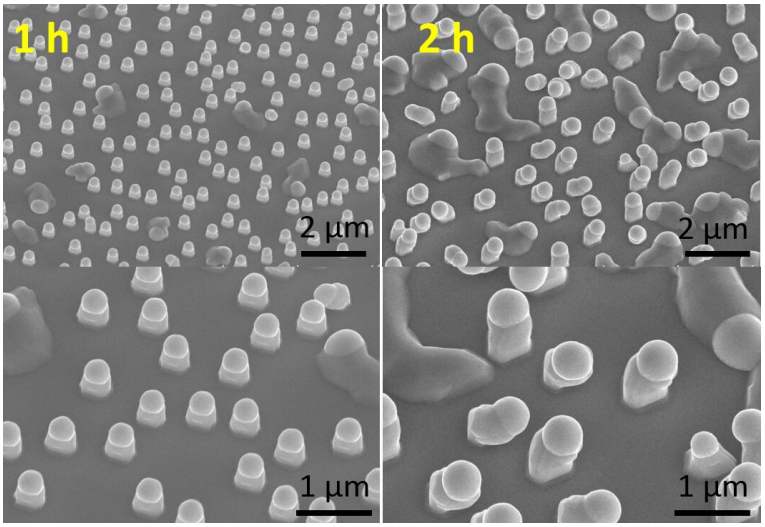


FIGURE 4.9: SEM images of Time series. The values of time is displayed on top left images in yellow fonts. The 1 hour sample is reference sample chosen. All images were taken on InSb {111}A substrates in central parts by SEM with the sample tilted 30°. The second row images are magnified from top row images. Scale bars are shown at right bottom on each images.

what Lin [21] has observed in self-seeded InSb nanowires growth by MOCVD. Lin [21] proved that in constant indium rich conditions, both indium droplets (particles) and nanowires (nano-pillars in article) grew in size as time increase. Table 4.2 shows particle diameter increases from about 403 nm in 1 h to 574 nm in 2 h, while nanowires length increase fron 376 nm in 1 h to 1118 nm in 2 h approximately. Similarly, in self-seeded InSb nanowires growth by MOVPE [22], the length and diameter of nanowires increase monotonically with growth time (10 min at diameter 173±20 nm and length 421±50 nm; 80 min at diameter 327± 42 nm and length 1272±59 nm). However, a confusing outcome is that the density of nanowires decreases a lot from 1 h growth to 2 h growth. Thus, it is necessary to understand why these phenomenon happen.

## 4.2 Tin particle formation on InSb {111} substrates

In this section, we tried to reproduce the Sn particle samples in order to investigate the size of Sn particles before nanowire growth. Eventually, we want to compare the particle sizes before and after nanowire growth. At the same time, we also want to find conditions to form smaller Sn particles before nanowire growth. We would use these smaller Sn particles to grow InSb nanowires for the sake of decreasing the nanowires diameters.

### 4.2.1 Time series and TESn flow series

The effect of Sn particle growth time on InSb {111}A substrate is displayed in Figure 4.10. As the Sn particles grow from 150 second to 900 second, slightly larger particles form while the density decreases. This could also be verified by Figure 4.11 and Figure 4.12. The reason for this phenomenon can be explained by two aspects. One

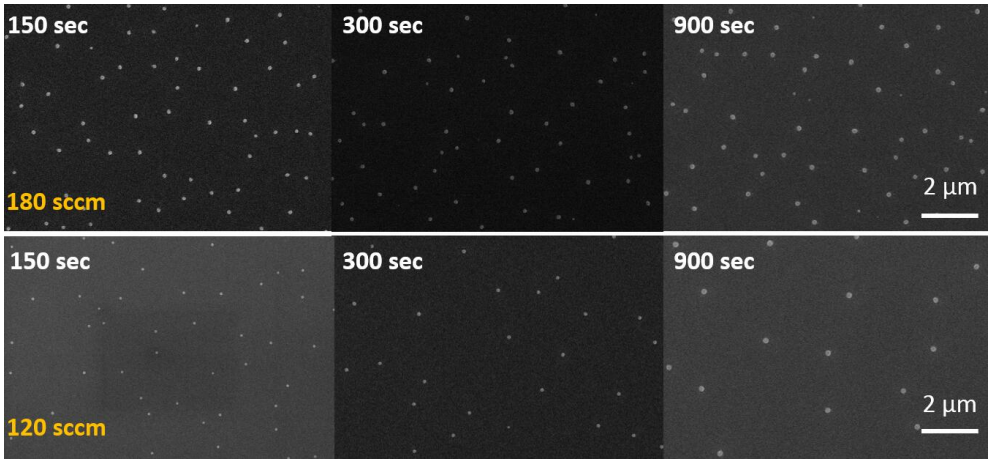


FIGURE 4.10: Top view SEM images of Sn particles grown on InSb {111}A substrate with increasing time. The TESn flow was $3.6 \times 10^{-9}$ mol/min (180 sccm) in the top row and and $2.3 \times 10^{-9}$ mol/min (120 sccm) in the bottom row. Scale bars are shown at right bottom on each images.

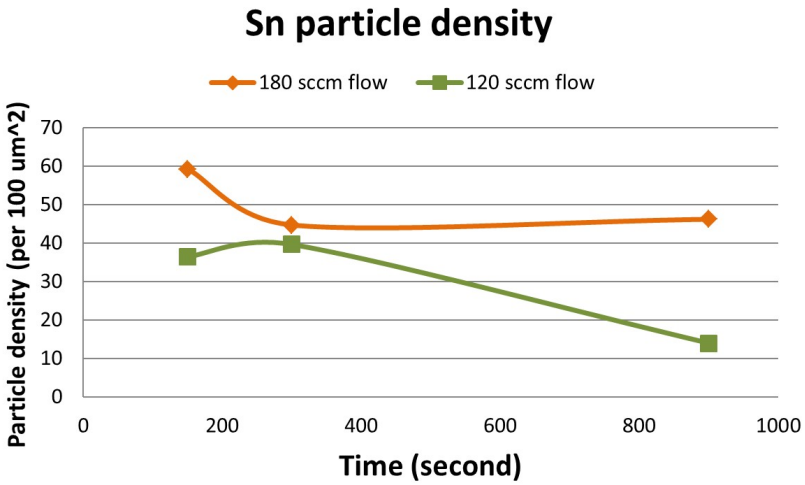


FIGURE 4.11: Data of Sn particle density. Orange and green squares are measured experimental data. Orange curve is the average value of Sn particle density with TESn flow at $3.6 \times 10^{-9}$ mol/min (180 sccm). Green curve is the average value of Sn particle density with TESn flow at $2.3 \times 10^{-9}$ mol/min (120 sccm). Orange and green curves are guides for the eyes.

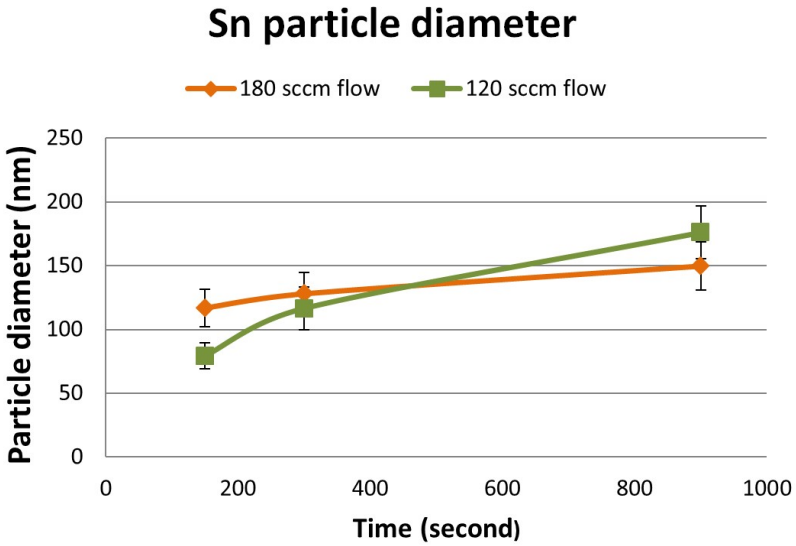


FIGURE 4.12: Data of Sn particle diameter. Orange and green squares are measured experimental data. Orange curve is the average value of Sn particle diameter with TESn flow at $3.6 \times 10^{-9}$ mol/min (180 sccm). Green curve is the average value of Sn particle diameter with TESn flow at $2.3 \times 10^{-9}$ mol/min (120 sccm). Orange and green curves are guides for the eyes.

is that longer growth time means that more materials are supplied, so that the Sn particles have more time to collect materials and form bigger particles. The other is the Ostwald ripening effect which is described in Chapter 2.

The amount of TESn source flow can also have effect on the Sn particle formation on InSb {111}A substrate. We can compare the differences in the first and second row images in Figure 4.10. The density of the first row images with TESn source flow equal to $3.6 \times 10^{-9}$ mol/min is larger than the density of the second row images with TESn source flow equal to $2.3 \times 10^{-9}$ mol/min. Figure 4.11 also gives this trend. The density of the Sn particles is decrease as time increases. There is a slight increase of density as time increases (orange curve from 400 seconds to 900 seconds). However, the diameter trend seems to increase linearly with respect to the growth time as shown in Figure 4.12. It should be noticed that the Sn particle diameter is a little bit larger at 900 seconds with TESn source flow at $2.3 \times 10^{-9}$ mol/min. This can be explained if we combine the diameter with density. At the same condition, the density is much lower which can explain the larger value for Sn particle sizes at $2.3 \times 10^{-9}$ mol/min grown in 900 seconds.

### 4.2.2 Tin particle size comparison

The growth conditions for particle formation are the same in Figure 4.13 a) and b). The parameters are TESn source flow at $3.6 \times 10^{-9}$ mol/min, growth time at 900 seconds, temperature at $409°C$. Figure 4.13 b) is also the reference sample. Through the statistics in Table 4.3, we detect an obvious difference. The particle sizes increase by more than 2 times after the nanowires growth. This could be explained by that the seed particle

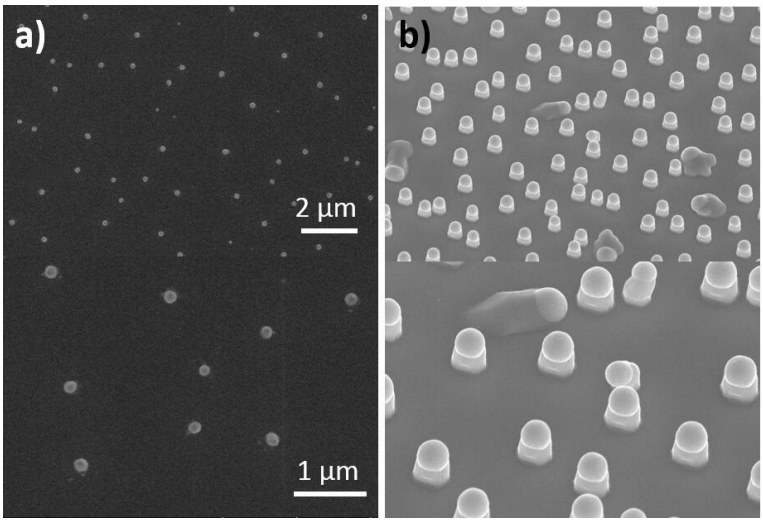


FIGURE 4.13: Particle size comparison before and after nanowire growth. Top view SEM images of Sn particle formation sample in a). After nanowires growth, $30^{\circ}$ tilted SEM images are given in b). All images were taken on InSb {111}A substrates in central parts. The second row images are magnified from top row images.

TABLE 4.3: Particle size comparison before and after nanowire growth

| Image NO. | Particle diameter | Particle density | NW length |
|---|---|---|---|
| Figure 4.13 a) | 150± 19 nm | 46 ( $/100\mu m^2$) | — |
| Figure 4.13 b) | 403± 68 nm | 103 ( $/100\mu m^2$) | 376± 48 nm |

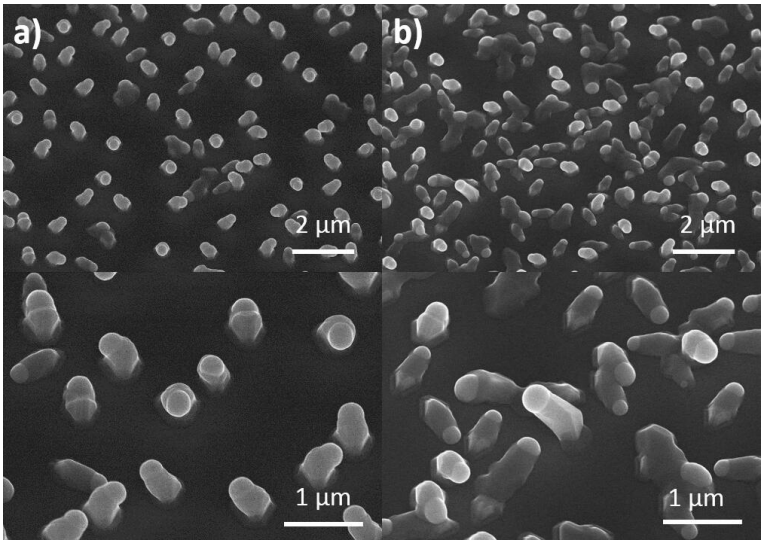


FIGURE 4.14: 30° tilted SEM images of smaller particle growth on InSb {111}A substrate. Nanowires growth conditions are the same in a) and b). The difference is between particle sizes. a). The particle conditions are TESn = $3.6 \times 10^{-9}$ mol/min, growth time t=900 seconds. b). The particle conditions are TESn = $2.3 \times 10^{-9}$ mol/min, growth time t=150 seconds. The scale bars are shown in the right bottom of each images.

collect growth species (In atoms or Sb atoms) to form alloy in order to reach the condition of supersaturation during InSb nanowires growth. However, the most interesting thing is that the particle density increases by nearly 2 times after nanowire growth. It is clear that there is almost $100\%$ Sn component in the particles before nanowire growth. After nanowires growth, the size of seed particles (Figure 4.13 b)) become much bigger which can be explained by metal alloy during the nanowires growth. However, the increasing of seed particle density after growth is confusing. The answer is found out after XEDS characteristic (See section 4.3.2).

### 4.2.3 Growth with smaller Sn particle size

We grew a sample with smaller particle sizes in order to examine if there is an effect of particles sizes on the nanowires growth. The nanowires growth conditions are the same for samples Figure 4.14 a) and b). The growth parameters are temperature at $420°C$, TMIn source flow at $9.5 \times 10^{-10}$ mol/min, TMSb source flow at 30 sccm, V-III ratio at 100, growth time at 1 hour. The morphology of nanowires under these conditions is mostly inclined but the wires are longer. The particle formation conditions of most samples are the same as in Figure 4.14 a), which are TESn = $3.6 \times 10^{-9}$ mol/min, growth time t=900 seconds. This also refers to Figure 4.10 the first row rightmost image. The smaller particle conditions are TESn = $2.3 \times 10^{-9}$ mol/min, growth time t=150 seconds, which also refers to Figure 4.10 the second row leftmost image. As shown in Figure 4.11 and Figure 4.12, the particle diameter of Figure 4.14 a) is about 150 nm and about 70 nm for Figure 4.14 b). There is no big difference between the density of particles in these two samples. The result shown in Figure 4.14 b) is that with smaller particles there is no significantly effect on nanowires growth.

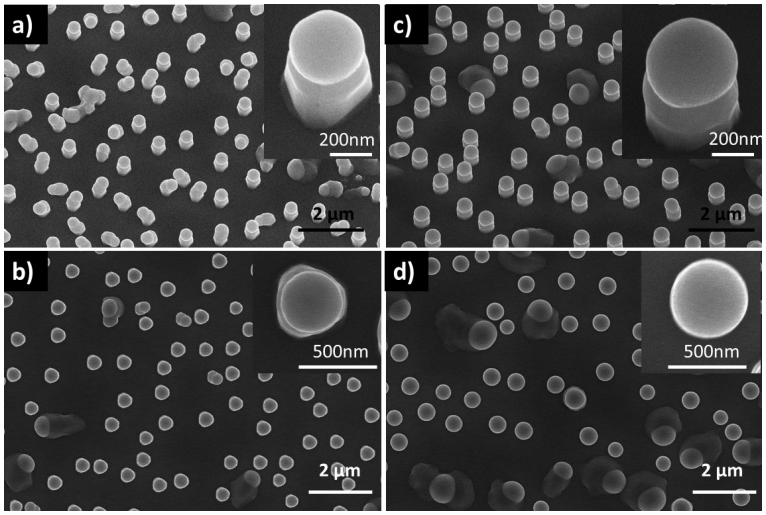


FIGURE 4.15: SEM images of Sn seeded InSb nanowires grown on InSb {111}A substrate. a) was taken in the center of the sample with 30° tilted SEM. c) was taken in the edge of the sample with 30° tilted SEM. b) and d) are the top view images from center and edge of the sample respectively. The insets show high-magnification SEM images of those nanowires. The scale bars are shown in the right bottom of each images.

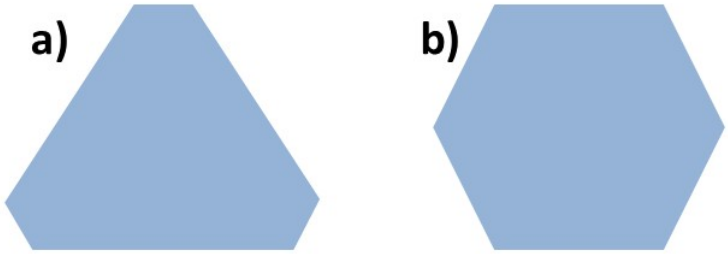


FIGURE 4.16: Sketch of sectional view of nanowire morphology along axial direction. a) is the center shape of the nanowires corresponding to Figure 4.15 a) and b). b) is the edge shape of the nanowires corresponding to Figure 4.15 c) and d).

## 4.3 Tin seeded InSb nanowire morphology and composition

### 4.3.1 Nanowires morphology

Figure 4.15 displays the reference sample. Figure 4.15 a) and b) are SEM images from centre of the sample with 30° tilted and top view respectively. The inset shows high magnification SEM image of one of those nanowires. Both the side and top view of the nanowires indicate a triangular base morphology. Although it is a triangular base morphology in general, it is a hexagonal shape in fact. Figure 4.16 a) provides a sketch of a sectional view of the nanowires along growth direction.

In contrast, Figure 4.15 c) and d) are SEM images from the edge of the sample with 30° tilted and top view respectively. The inset show high magnification SEM image of

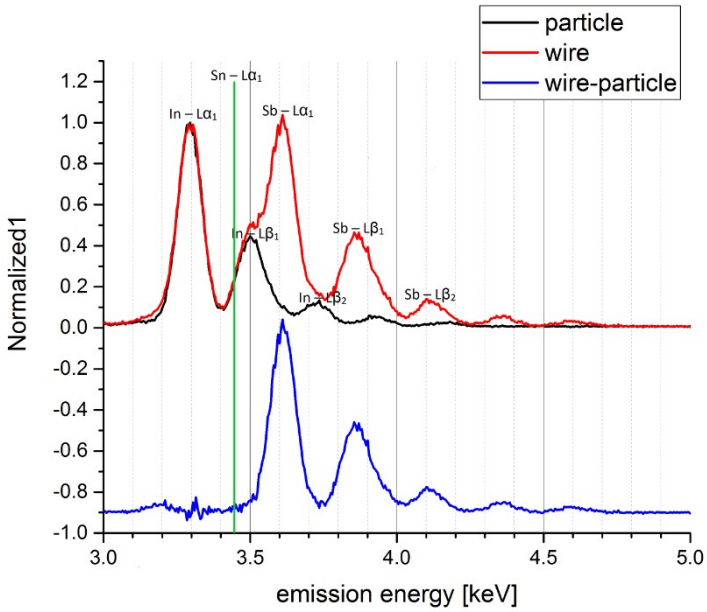


FIGURE 4.17: XEDS characteristic of Sn seeded InSb nanowires. The horizontal (X) axis is the emission energy. The vertical (Y) axis is the intensity being detected. Red and black curves are X-ray emission spectrum for the nanowire and seed particle respectively. By subtracting spectrum of particle from the spectrum of wire, it results in blue spectrum. The vertical green line signifies the intensity maximum of the Sn emission energy marked for distinguishing the signal.

TABLE 4.4: Element Identification by XEDS in FSEM

| Element | Atomic% in particle | Atomic% in nanowire |
|---|---|---|
| In | 78± 11 | 60 ± 12 |
| Sb | 21± 11 | 40 ± 12 |
| Sn | 1± 1 | 0 |

one of those nanowires. Side view indicates a hexagonal morphology while it is hard to see the morphology from the top view because of the huge seed particles. Figure 4.16 b) provides a sketch of a sectional view of the nanowires along the growth direction. Particles are not perfectly round both in center and edge of the sample.

As shown in Figure 4.4 and Figure 4.5, the TMIn source flow effects both the size of seed particles and the length of the nanowires. The TMSb source flow on the other hand has much influence on the length and orientation of nanowires but not on the seed particles as shown in Figure 4.6 and Figure 4.7. In conclusion, the V-III ratio plays an important role on the morphology of nanowires. This is agreed with what Lin [21] has demonstrated on self-seeded InSb nanocryatal growth.

TABLE 4.5: Element Identification by XEDS in TEM

| Element | Atomic% in particle | Atomic% in nanowire |
|---|---|---|
| In | 101± 1 | 51 ± 1 |
| Sb | 3± 1 | 49 ± 1 |
| Sn | -3± 3 | 0± 3 |

### 4.3.2 Nanowires composition

Around 10 nanowires (including particles) from the reference sample are analysed by XEDS in a Field Emission Scanning Electron Microscopy (FSEM) with both point and map scanning. About 4 nanowires from reference sample are analysed by XEDS in a TEM with both point and map scanning. We did not detect any Sn inside the particle or nanowire stem in any of the XEDS measurements (Table 4.4 and Table 4.5). Instead, we found almost 100% In in the seed particle. In, Sn and Sb are near each other with atomic number 49, 50, 51 respectively in the periodic table of elements. Thus, it may be hard for the detectors of XEDS to distinguish the signals among these three elements since their emission energies are too close. In other words, there could be overlap between these signals. The green vertical line in Figure 4.17 points out the intensity maximum signal of Sn. However, at this energy there is no hint of a 'shoulder' from overlapping signals.

We obtained only Sb signal (Figure 4.17 blue curve) with nanowire stem signal (Figure 4.17 red curve) minus particle signal (Figure 4.17 black curve). There is indeed a significant amount of In in the particle. There should be some amount of Sb (21% in Table 4.4) inside the seed particle but at the bottom of the particle close to top stem of nanowire. The reason that we did not detect Sb by using XEDS in TEM could be that we only scanned the top part of the particle which was far from the interface area between the particle and the nanowire stem. In self-seeded InSb nanowires growth by MOVPE [22], In–Sb particles on top reveals a temporal dependence of their chemical composition (Grow 40 min, 20 at.% Sb and Grow 20 min 7–8 at.% Sb). The composition of nanowire stem were measured approximately half amount In and half amount Sb (Table 4.4 and Table 4.5). From the previous study, antimonide nanowires prefer ZB crystal structure formation [14]. The structure of InSb nanowires in this project could be ZB, but we did not confirm by TEM measurements. In self-seeded InSb nanowires growth by MOVPE [22], there was a transitions from pure ZB structure at the beginning to pure Wurtzite structure at the end.

Finally, we could conclude that Sn seeded InSb nanowires become self-seeded (In seeded) InSb nanowires growth. This is supported by the following results. First, the density of seed particle changes a lot before and after nanowire growth (Figure 4.13 and Table 4.3). Second, there is no significant effect on the growth from the smaller particles (Figure 4.14). Third, there is no Sn identified by XEDS (Table 4.4 and Table 4.5). However, due to the limitation of the equipment, the overlap signal between In, Sb and Sn is hard to distinguish, thus there could be exist some Sn inside particle.

Thus, this is a self-seeded InSb nanowires growth case. However, one should be aware that the XEDS characteristic of nanowires (including particles) composition is measured after nanowires cooling down. There are some composition changes during

cooling down, but here we assume that this after-growth composition is approximately equal to the composition during growth. Indium seed particles play an essential role in the dynamics of nanowires growth. Specifically, the size and shape of the seed particles mainly determine the diameter of the nanowires. According to Figure 4.4 and Figure 4.5, indium has a tendency to accumulate in the particles.

In the widely used gold seeded InSb nanowires growth, the most common phase of the particle is $AuIn$ or $AuIn_2$ [18] [70] [68]. It is believed that nanowire growth typically occurs along pseduo-binary-tie-lines according to Au-In-Sb ternary phase diagram [14]. Similarly, tie-lines do not exist in the In-Sb-Sn phase diagram because there are no In-Sb phases at growth temperature see (Figure 2.4). There do not exist this tie-lines in Sn-In-Sb ternary phase diagram (Figure 2.4). This may be the reason why high amount of indium is inside the seed particle.

How do the Sn particles effect on the InSb nanowires growth? Where does the Sn go? Around these questions, we did comparable InSb nanowires growth without Sn seed particles. The results show much more inclined InSb nanowires (almost no vertical InSb nanowires) compared with the reference sample (Figure 4.15). We conclude that Sn-seed particles help nucleation and affect the InSb NWs growth. The Sn seeded InSb nanowire growth should result in mixed Sn seeded and In seeded InSb nanowire growth. The amount of In inside the seed particle is large and In particles are very easily formed on both substrate A and B according to our experiments. There are several reasons. First, the formation of indium particles could be related to the surface reconstruction of substrates. As discussed in the theory part, indium particles were found on both InSb {111}A and InSb {111}B substrates. For gold-seeded InSb nanowires grown by MOVPE, indium droplets were also found on the InAs (111)B substrate. Second, as the indium particle is in liquid phase, the surface of this liquid particle has a large accommodation coefficient and readily collects growth species (In atoms and Sb atoms). Third, the continuous supply of TMIn source during nanowires growth. The rate of source flow is faster than the rate of nanowires growth, which makes seed particles much bigger.

In this project, we think that the accomulation of indium particles continue during InSb nanowires growth. Even after indium particle reaching the supersaturation conditions, it continues to collect growth species (In atoms and Sb atoms) both during nanowires growth and particle growth. Further more, the nanowires radial growth occur at the same time. This is referred to nanowires facets (sidewall) growth or Vapour-Solid growth. The reason for this could be the surface structure of nanowires facets which are favourable for nanowires growth. For example stacking fault, defects, steps, twinning or others on the side-facets of nanowires could make the surface rough, leading to increased incorporation.

## 4.4 Mass transport modelling

In this section, we aim to describe the evolution of the nanowires morphology versus the source flow of precursors (TMIn and TMSb). A mass transport model is built under the assumptions based on the obtained experimental data.

In Figure 2.1, the schematic of nanowires growth and the hypothesis of this growth model are shown. We assume the nanowire to have the shape of a cylinder and the seed particle to have the shape of a hemisphere. $R$ is the radius of the nanowire and

the seed particle. We suppose the diameter is the same between the nanowires stem and the particle. $H$ is the nanowire height (excluding the particle). $L$ is the diffusion length of adatoms. In this project, we assume that the adatoms diffusion length ($L$) is larger than the total height ($R + H$) from Figure 2.1. The reasons are that the growth rate is very low and nanowires are very short (small $H$) and fat (large $R$) compared to many other materials system. We assume that the flux $j$ (in unit of sccm) of precursors arrives uniformly on the surfaces of nanowire and substrate. Adsorbed atoms can diffuse freely in the range of their diffusion length $L$. Adatoms that impinge on the seed particle (surface area (1)) could contribute to particle growth or nanowire axial growth or radial growth. Similarly, adatoms on the nanowire sidewall facets (surface area (2)) and on the substrate (surface area (3)) could also contribute to particle growth or nanowire axial growth or radial growth. The three different surface areas are:

Surface area (1): $2\pi R^2$

Surface area (2): $2\pi RH$

Surface area (3): $\pi(R + L)^2 - \pi R^2 = \pi L(2R + L)$

These three different surface areas are the total collection area of materials coming from vapor phase which contribute to nanowire growth. There are also some other hypothesis considered in this growth model. The InSb film growth on the substrate is neglected. Competition for material between different nanowires is neglected, meaning that the interspacing of nanowires is large. Seed particle and cylinder nanowire will increase over time.

We give the sum of three different surface areas ($A$): $A = 2\pi R^2 + 2\pi RH + \pi L(2R + L)$ . And then A is divided into three different parts with different ratios $a$, $b$ and $c$ respectively ($0 < a, b, c < 1$). $aA$ is for particle growth. $bA$ is for axial growth of nanowires stem. $cA$ is for radial growth of nanowires stem. For constrains, the relation of $a$, $b$ and $c$ is:

$$a + b + c = 1 \tag{4.1}$$

Through the above considerations, the variation in the seed particle volume per unit time is simply given by:

$$\frac{dV(particle)}{dt} = j_{tot} \cdot aA \tag{4.2}$$

The volume of hemisphere particle is given by:

$$V(particle) = \frac{2}{3} \cdot \pi R^3 \tag{4.3}$$

Similarly, the nanowire axial growth is expressed by the variation in nanowire (exclude seed particle) volume per unit time caused by height ($H$) increase:

$$\frac{dV(axial)}{dt} = j_{tot} \cdot bA \tag{4.4}$$

And the nanowire radial growth is expressed by the variation in nanowire (exclude seed particle) volume per unit time caused by diameter ($2R$) increase:

$$\frac{dV(radial)}{dt} = j_{tot} \cdot cA \tag{4.5}$$

The volume of particle is easy to calculate (equ.(4.3)). However, the increasing volume caused by axial growth ($dV(axial)$) and increasing volume caused by radial growth ($dV(radial)$) are not known. It is hard to distinguish from the experimental results. However, the volume of nanowire stem ($V(NWstem)$, excluding seed particle), which is equal to the cylinder volume can be calculated. We have the relation between these volumes:

$$dV(axial) + dV(radial) = dV(NWstem) \tag{4.6}$$

The volume of cylinder nanowires stem is given by:

$$V(NWstem) = \pi R^2 H \tag{4.7}$$

$j_{tot}$ is the total flow of precursors. In equation (4.2), (4.4) and (4.5), the right most term $A$ is total collection area for reaction materials with three different surface areas mentioned in Figure 2.1, and $t$ refers the nanowires growth time.

If we take a ratio between equation (4.2) and (4.4) plus (4.5), it will lead to a simplified expression for the relationship between nanowire height ($H$) and radius ($R$):

$$\frac{R}{H} = \frac{a}{1-a} \tag{4.8}$$

and $j_{tot}$ is given by:

$$j_{tot} = \frac{1}{t}\int_0^R \frac{2R^2}{2R^2 + 2aLR + aL^2} dR \tag{4.9}$$

After seed particle (Sn) formation, the TESn source is closed and InSb nanowire growth will take place. The available sources for growth are TMIn and TMSb. The growth species will be the In and Sb atoms resulting from the decomposition of TMIn and TMSb. During this complex growth process, many will affect the growth, such as chemical reactions, phase transformation, diffusion, surface processes and mass transport. The rate limiting steps of nanowire growth can be the mass transport process from vapor phase to solid phase. The pyrolysis of precursors can also determine the growth rate. According to the scientific references, TMIn can decompose completely at growth temperature $420°C$, while only half of TMSb can decompose [61] [63] [62]. The ratio of In atoms and Sb atoms can also affect the InSb nanowires growth. In this modelling, $\alpha$ and $\beta$ represent the ratios of source flow (TMIn and TMSb respectively) contributing to InSb nanowires growth. In the ideal case, one needs 50% In atoms and 50% Sb atoms to form InSb nanowire structure. However, if this balance is broken, the growth rate will be limited by the smaller one. Normally, it is hard to reach the ideal case. It should be noted that there are also other limiting steps. Through the above consideration, the relationship among the total flow ($j_{tot}$), TMIn flow ($j_{In}$) and TMSb flow ($j_{Sb}$) is given by:

$$\frac{1}{j_{tot}} = \frac{1}{\alpha j_{In}} + \frac{1}{\beta j_{Sb}} \tag{4.10}$$

where $j_{tot}$ is the effective total flow of precursors TMIn and TMSb. $j_{In}$ and $j_{Sb}$ are the TMIn source flow and TMSb source flow respectively. $\alpha$ and $\beta$represent the ratio of source flow (TMIn and TMSb respectively) contributing to InSb nanowires growth, $0 < \alpha, \beta < 1$. The reason is that not all the growth species arriving on the three available surfaces will contribute to the nanowire growth in the realistic experiment. Then

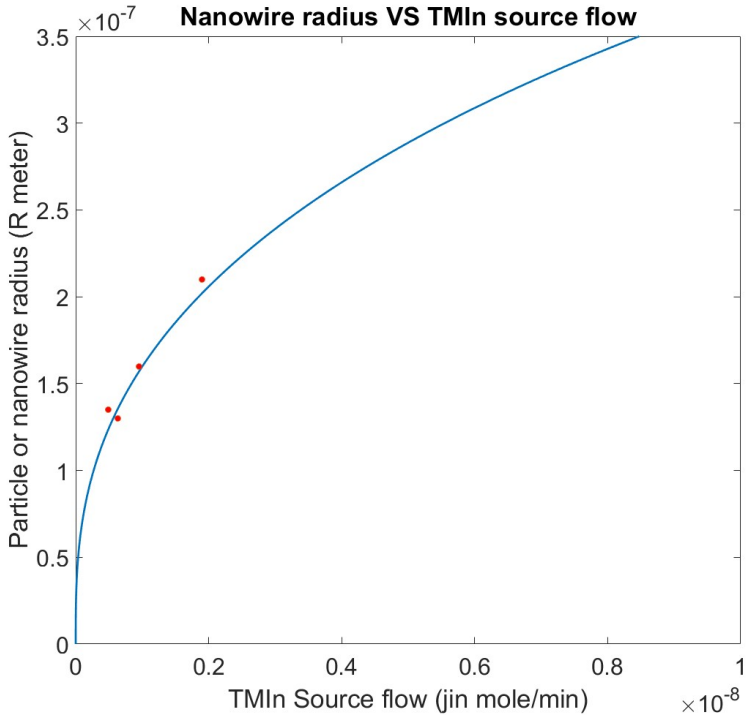


FIGURE 4.18: Mass transport modelling of TMIn series of InSb nanowires growth. $t = 600min$; $L = 1\mu m$; $j_{Sb} = 4.8 \times 10^{-8} mol/min$; $a = \frac{1}{3}$; $\beta = 0.01$; $\alpha = 0.011$

we could extract TMIn flow or TMSb flow from the total flow and generate the new solution modelling by combining equ.(4.9) and equ.(4.10):

$$\frac{\alpha j_{In} \cdot \beta j_{Sb}}{\alpha j_{In} + \beta j_{Sb}} = \frac{1}{t} \int_0^R \frac{2R^2}{2R^2 + 2aLR + aL^2} dR \tag{4.11}$$

In TMIn flow series of nanowires growth, according to the experimental data from Figure 4.4 and Figure 4.5, the estimated relation between the radius ($R$) of particle and the length ($H$) of Nanowires stem is $H = 2R$ approximately. Thus, we could obtain $a = \frac{1}{3}$ by equ.(4.8). By setting some certain values for the parameters, we calculate the TMIn source flow series as shown in Figure 4.18 blue line. The red dots are measured experimental data corresponding to Figure 4.5. Source incorporate ratio $\alpha$ can vary from certain range from 0 to 1 to fit the experimental growth tendency. This means that different ratios of TMIn sources will contribute to different growth rate. The MATLAB software is used for the calculation. The modelling fits the TMIn series well. However, for the TMSb series of InSb nanowires growth, this calculation does not give a good match. The most important reason could be that there is not much Sb inside the particle. There should be some modifications to the model to fit the TMSb source flow series.

# Chapter 5

# Conclusions and outlook

## 5.1 Conclusions

In summary, we have developed and understanding of Sn seeded InSb nanowires growth using MOVPE experiments and mass transport modelling. The VLS growth mechanism is the fundamental theory for nanowires synthesis. The In-Sb-Sn ternary phase diagram helps us to understand metal seeded III-V semiconductor nanowires growth in the view of thermodynamic.

The optimized growth temperature was found to be $420°C$. Due to sample edge effects, the morphology of nanowires (excluding the seed particle) is different between center and edge of the sample. In the center, the nanowires have a triangular base (Figure 4.16 a)). However, at the edge, the nanowires have a hexagonal base (Figure 4.16 b)). The particle diameters increase a lot from center to edge (Figure 4.2) when temperature rise. The length of nanowires are not very different between center and edge but increase as temperature goes high (Figure 4.3).

The nucleation and polarity of Sn-seeded InSb nanowires are more affected by V/III ratio than temperature. Particle size is strongly influenced by TMIn flow (Figure 4.5). The Sb amount is a key factor to control the morphology of nanowires as we could see from the TMSb series (Figure 4.7). It shows that the diameter of the particles and the length of the nanowires both decrease when the total flow is reduce to half (Figure 4.8).

The growth rate is low (Figure 4.9). From 1 hour to 2 hour growth, the nanowires change from vertical to more inclined wires. The growth direction for inclined wires is uncertain. Particle diameter increase can be explained by indium accumulation. The length of nanowires are more than doubled. Why the density decreases from 1 hour to 2 hour growth is still unknown.

The seed particle size increases much during nanowires growth, from about 150 nm to 403 nm (Table 4.2). There is no significant effect on particle size with smaller seed particles growth (Figure 4.14). X-EDS measurements show that no element at Sn is detected (Table 4.4 and Table 4.5). Combing the above results, we conclude that Sn seeded InSb nanowire growth become In seeded InSb nanowires growth. The mass transport modelling fits the experimental data of TMIn series much better than TMSb series. This helps us to understand how the radial and axial grow happen for InSb nanowires growth.

In order to investigate if the Sn particles have effect on the InSb nanowires growth, further experiments about InSb nanowires growth without Sn seed particle were run. The results show much more inclined InSb nanowires (almost no vertical InSb nanowires) compared with the reference sample (Figure 4.15). We conclude that Sn-seed particles help nucleation and affect the InSb NWs growth.

## 5.2 Outlook

Better growth conditions can potentially be achieved by tuning the V/III ratio especially in the TMSb series. The crystal structure of InSb nanowires can also be investigated by TEM for further study. As the nanowires are very 'fat' (large diameter), it is also a challenge to break off the nanowires for TEM sample preparation.

Several attempts with XEDS were made to check the particle composition. However since In, Sn, and Sb have overlapping signals, it is hard to quantify the particles composition. A better way can be considered to distinguish these elements. Further more, the mass transport modelling needs to be further developed to fit the TMSb series.

Understanding the difference between Sn seeded and self-seeded InSb nanowire growth needs much more efforts. Sn seed particle size comparison before and after nanowires growth can be achieved in the experiments with different time series (such as 5 min, 15 min, 30 min...) on the reference sample (Figure 4.15). According to the In-Sb-Sn ternary phase diagram, the SbSn solid phase along the Sn-Sb line can be a focus of consideration. In the particle droplet study, Sb can be added into the Sb droplets in order to reach the SbSn solid phase. In this case, a precursor flow of TMSb can be given together with Sn particle formation. The composition of droplets will be modified and this may lead to another story about InSb nanowires growth.

# Bibliography


1. Hnida, K., Mech, J. & Sulka, G. D. Template-assisted electrodeposition of indium–antimony nanowires–Comparison of electrochemical methods. *Applied Surface Science* **287,** 252–256 (2013).
2. Dick, K. A. A review of nanowire growth promoted by alloys and non-alloying elements with emphasis on Au-assisted III–V nanowires. *Progress in Crystal Growth and Characterization of Materials* **54,** 138–173 (2008).
3. Joyce, H. J. *et al.* III–V semiconductor nanowires for optoelectronic device applications. *Progress in Quantum Electronics* **35,** 23–75 (2011).
4. Shafa, M., Akbar, S., Gao, L., Fakhar-e Alam, M. & Wang, Z. M. Indium Antimonide Nanowires: Synthesis and Properties. *Nanoscale research letters* **11,** 1 (2016).
5. Dick, K. A. & Caroff, P. Metal-seeded growth of III–V semiconductor nanowires: towards gold-free synthesis. *Nanoscale* **6,** 3006–3021 (2014).
6. Mårtensson, E. In-situ MOVPE formation of alternative seed particles for nanowire growth (2015).
7. Zamchiy, A., Baranov, E. & Khmel, S. New approach to the growth of $SiO_2$ nanowires using Sn catalyst on Si substrate. *physica status solidi (c)* **11,** 1397–1400 (2014).
8. Sun, R. *et al.* Sn-seeded GaAs nanowires as self-assembled radial p–n junctions. *Nano letters* **15,** 3757–3762 (2015).
9. Tornberg, M. *et al.* Demonstration of Sn-seeded GaSb homo-and GaAs–GaSb heterostructural nanowires. *Nanotechnology* **27,** 175602 (2016).
10. Sareminia, G., Zahedi, F, Eminov, S. & Karamian, A. Cleaning method of InSb [111] B of n-InSb [111] A/B for the growth of epitaxial layers by liquid phase epitaxy. *Journal of Semiconductors* **32,** 056001 (2011).
11. Hulme, K. & Mullin, J. Indium antimonide—A review of its preparation, properties and device applications. *Solid-State Electronics* **5,** 211IN3–247IN10 (1962).
12. Kuo, C.-H., Wu, J.-M., Lin, S.-J. & Chang, W.-C. High sensitivity of middle-wavelength infrared photodetectors based on an individual InSb nanowire. *Nanoscale research letters* **8,** 1–8 (2013).
13. Paul, R. K., Badhulika, S. & Mulchandani, A. Room temperature detection of $NO_2$ using InSb nanowire. *Applied Physics Letters* **99,** 033103 (2011).
14. Borg, B. M. & Wernersson, L.-E. Synthesis and properties of antimonide nanowires. *Nanotechnology* **24,** 202001 (2013).
15. Plissard, S. S., Bakkers, E. E., Frolov, S., Kouwenhoven, L., *et al.* Quantized conductance in an InSb nanowire. *Nano Letters* **13,** 387 (2013).

16. Kuo, C.-H., Wu, J.-M. & Lin, S.-J. Room temperature-synthesized vertically aligned InSb nanowires: electrical transport and field emission characteristics. *Nanoscale research letters* **8,** 1–8 (2013).

17. Paul, R. K. *et al.* Chemical vapor deposition and electrical characterization of sub-10nm diameter InSb nanowires and field-effect transistors. *Materials Chemistry and Physics* **121,** 397–401 (2010).

18. Caroff, P. *et al.* High-Quality InAs/InSb Nanowire Heterostructures Grown by Metal–Organic Vapor-Phase Epitaxy. *Small* **4,** 878–882 (2008).

19. Nilsson, H. A. *et al.* Temperature dependent properties of InSb and InAs nanowire field-effect transistors. *Applied Physics Letters* **96,** 153505 (2010).

20. Gorji Ghalamestani, S. *et al.* Demonstration of Defect-Free and Composition Tunable $Ga_xIn_{1-x}Sb$ Nanowires. *Nano letters* **12,** 4914–4919 (2012).

21. Lin, A., Shapiro, J. N., Eisele, H. & Huffaker, D. L. Tuning the Au-Free InSb Nanocrystal Morphologies Grown by Patterned Metal–Organic Chemical Vapor Deposition. *Advanced Functional Materials* **24,** 4311–4316 (2014).

22. Mandl, B. *et al.* Crystal structure control in Au-free self-seeded InSb wire growth. *Nanotechnology* **22,** 145603 (2011).

23. Ngo, C. *et al.* Effect of precursor flux on compositional evolution in $InP_{1-x}Sb_x$ nanowires grown via self-catalyzed vapor–liquid–solid process. *Journal of Crystal Growth* **336,** 14–19 (2011).

24. Sapkota, G. & Philipose, U. Synthesis of metallic, semiconducting, and semi-metallic nanowires through control of InSb growth parameters. *Semiconductor Science and Technology* **29,** 035001 (2014).

25. Magnano, E. *et al.* Growth morphology and electronic properties of Sn deposited on different InSb surfaces. *Surface science* **433,** 387–391 (1999).

26. Wallentin, J. & Borgström, M. T. Doping of semiconductor nanowires. *Journal of Materials Research* **26,** 2142–2156 (2011).

27. Chen, Y., Jiang, J, Wang, B & Hou, J. Synthesis of tin-doped indium oxide nanowires by self-catalytic VLS growth. *Journal of Physics D: Applied Physics* **37,** 3319 (2004).

28. Gutsche, C. *et al.* n-type doping of vapor–liquid–solid grown GaAs nanowires. *Nanoscale Res Lett* **6,** 1 (2010).

29. Terra, F *et al.* Fabrication, investigation, and application of doped indium antimonide microcrystals in radiation-resistant sensors. *Russian physics journal* **46,** 601–608 (2003).

30. Chen, W. *et al.* Incorporation and redistribution of impurities into silicon nanowires during metal-particle-assisted growth. *Nature communications* **5** (2014).

31. Yu, L. *et al.* Plasma-enhanced low temperature growth of silicon nanowires and hierarchical structures by using tin and indium catalysts. *Nanotechnology* **20,** 225604 (2009).

32. Chockla, A. M., Klavetter, K. C., Mullins, C. B. & Korgel, B. A. Tin-seeded silicon nanowires for high capacity Li-ion batteries. *Chemistry of Materials* **24,** 3738–3745 (2012).

33. Jeon, M. & Kamisako, K. Synthesis and characterization of silicon nanowires using tin catalyst for solar cells application. *Materials Letters* **63,** 777–779 (2009).
34. Kumar, R. R., Rao, K. N., Rajanna, K & Phani, A. Growth of tin catalyzed silicon nanowires by electron beam evaporation. *Adv Mater Lett* **4,** 836–840 (2013).
35. Pohl, U. W. in *Epitaxy of Semiconductors* 1–9 (Springer, 2013).
36. Johansson, J., Svensson, C. P. T., Mårtensson, T., Samuelson, L. & Seifert, W. Mass transport model for semiconductor nanowire growth. *The Journal of Physical Chemistry B* **109,** 13567–13571 (2005).
37. Dubrovskiĭ. The role of surface diffusion of adatoms in the formation of nanowire crystals.
38. Jensen, L. E. *et al.* Role of surface diffusion in chemical beam epitaxy of InAs nanowires. *Nano Letters* **4,** 1961–1964 (2004).
39. Dayeh, S. A., Yu, E. T. & Wang, D. Surface diffusion and substrate- nanowire adatom exchange in InAs nanowire growth. *Nano letters* **9,** 1967–1972 (2009).
40. Persson, A. I., Fröberg, L. E., Jeppesen, S., Björk, M. T. & Samuelson, L. Surface diffusion effects on growth of nanowires by chemical beam epitaxy. *Journal of Applied Physics* **101,** 034313 –N.PAG. ISSN: 00218979 (2007).
41. Fröberg, L., Seifert, W. & Johansson, J. Diameter-dependent growth rate of InAs nanowires. *Physical Review B* **76,** 153401 (2007).
42. Marqusee, J. & Ross, J. Theory of Ostwald ripening: Competitive growth and its dependence on volume fraction. *The Journal of chemical physics* **80,** 536–543 (1984).
43. Gentry, S. T., Kendra, S. F. & Bezpalko, M. W. Ostwald ripening in metallic nanoparticles: stochastic kinetics. *The Journal of Physical Chemistry C* **115,** 12736–12741 (2011).
44. Alloyeau, D *et al.* Ostwald ripening in nanoalloys: when thermodynamics drives a size-dependent particle composition. *Physical review letters* **105,** 255901 (2010).
45. Bastús, N. G., Comenge, J. & Puntes, V. Kinetically controlled seeded growth synthesis of citrate-stabilized gold nanoparticles of up to 200 nm: size focusing versus Ostwald ripening. *Langmuir* **27,** 11098–11105 (2011).
46. Wagner, R. & Ellis, W. Vapor-liquid-solid mechanism of single crystal growth. *Applied Physics Letters* **4,** 89–90 (1964).
47. Givargizov, E. Fundamental aspects of VLS growth. *Journal of Crystal Growth* **31,** 20–30 (1975).
48. Wacaser, B. A. *et al.* Preferential interface nucleation: an expansion of the VLS growth mechanism for nanowires. *Advanced Materials* **21,** 153–165 (2009).
49. Plante, M. C. & LaPierre, R. R. Analytical description of the metal-assisted growth of III–V nanowires: axial and radial growths. *Journal of Applied Physics* **105,** 114304 (2009).
50. Ghasemi, M. *Thermodynamic modeling of the materials systerms for nanowires: CALPHAD, DFT and experiments* PhD thesis (Lund University, 2016).
51. Wever, J *et al.* A new type of reconstruction on the InSb (111) surface determined by grazing incidence X-ray diffraction. *Surface science* **321,** L225–L232 (1994).

52. Mishima, T. & Osaka, T. Profile imaging of the InSb {111} A, B-(2× 2) surfaces. *Surface science* **395,** L256–L260 (1998).

53. Ohtake, A. & Nakamura, J. Reflection high-energy electron diffraction analysis of the InSb {111} A, B-(2× 2) surfaces. *Surface science* **396,** 394–399 (1998).

54. Bohr, J *et al.* Model-independent structure determination of the InSb (111) 2× 2 surface with use of synchrotron x-ray diffraction. *Physical review letters* **54,** 1275 (1985).

55. Eguchi, T. *et al.* Structures and electronic states of the InSb{1 1 1}A,B-(2×2) surfaces. *Surface Science* **514,** 343 –349. ISSN: 0039-6028 (2002).

56. Nishizawa, M., Eguchi, T., Omoto, S.-i. & Osaka, T. STM study of the InSb (111) A-(2× 6) surface. *Applied surface science* **121,** 204–207 (1997).

57. Nishizawa, M., Eguchi, T., Misima, T., Nakamura, J. & Osaka, T. Structure of the InSb (111) A-($2\sqrt{3} \times 2\sqrt{3}$)- R 30° surface and its dynamical formation processes. *Physical Review B* **57,** 6317 (1998).

58. Proessdorf, A *et al.* The physical origin of the InSb (111) A surface reconstruction transient. *Surface Science* **606,** 1458–1461 (2012).

59. Nakada, T, Ikeda, T, Yata, M & Osaka, T. In-situ observation of the polar InSb (111) reconstructed surface by ultra high vacuum reflection electron microscopy. *Surface Science* **222,** L825–L830 (1989).

60. Björkqvist, M., Olsson, M. G. & Karlsson, J. K. O. InSb(1 1 1 ) New surface reconstruction. *Journal of Vacuum Science Technology B, Nanotechnology and Microelectronics: Materials, Processing, Measurement, and Phenomena* **14,** 957–960 (1995).

61. Buchan, N., Larsen, C. & Stringfellow, G. Mass spectrometric studies of trimethylindium pyrolysis. *Journal of Crystal Growth* **92,** 591–604 (1988).

62. Larsen, C., Li, S. & Stringfellow, G. Decomposition mechanisms of trimethylantimony and reactions with trimethylindium. *Chemistry of Materials* **3,** 39–44 (1991).

63. Larsen, C. & Stringfellow, G. Decomposition kinetics of OMVPE precursors. *Journal of crystal growth* **75,** 247–254 (1986).

64. Laurenius, L. Epitaxial growth of Sn seeds and Sn-seeded InSb nanowires on InSb substrates (2015).

65. Goldstein, J. *et al. Scanning electron microscopy and X-ray microanalysis: a text for biologists, materials scientists, and geologists* (Springer Science & Business Media, 2012).

66. Williams, D. B. & Carter, C. B. *Transmission electron microscopy: a textbook for materials science* 2009.

67. Mandl, B. *et al.* Growth mechanism of self-catalyzed group III- V nanowires. *Nano letters* **10,** 4443–4449 (2010).

68. Caroff, P. *et al.* InSb heterostructure nanowires: MOVPE growth under extreme lattice mismatch. *Nanotechnology* **20,** 495606 (2009).

69. Du, W.-N. *et al.* The self-seeded growth of InAsSb nanowires on silicon by metal-organic vapor phase epitaxy. *Journal of Crystal Growth* **396,** 33–37 (2014).

70. Plissard, S. R. *et al.* From InSb nanowires to nanocubes: looking for the sweet spot. *Nano letters* **12,** 1794–1798 (2012).